Waste valorization as low-cost media engineering for Auxin production from the newly isolated *Streptomyces rubrogriseus* AW22: Model development

Wiem Alloun[a,*], Mohammed Berkani[b,*], Akila Benaissa[c], Amin Shavandi[d], Maroua Gares[a], Camellia Danesh[e,*], Dalloula Lakhdari[b], Noreddine Kacem Chaouche[a]

[a] Laboratory of Mycology, Biotechnology and Microbial Activity (LaMyBAM), Department of Applied Biology, Constantine 1 University, BP, 325, Aïn El Bey, Constantine 25017, Algeria

[b] Biotechnology Laboratory, National Higher School of Biotechnology, Ali Mendjeli University City, BP E66, 25100 Constantine, Algeria

[c] Pharmaceutical Research and Sustainable Development Laboratory (ReMeDD), Department of Pharmaceutical Engineering, Faculty of Process Engineering, Constantine 3 University, Constantine 25000, Algeria

[d] 3BIO-BioMatter Unit, École Polytechnique de Bruxelles, Université Libre de Bruxelles (ULB), Avenue F.D. Roosevelt, 50-CP 165/61, 1050 Brussels, Belgium

[e] The University of Johannesburg, Department of Chemical Engineering, P.O. Box 17011, Doornfontein 2088, South Africa

Corresponding Authors
[*]wiemalloun@gmail.com (W. Alloun);
[*]m.berkani@ensbiotech.edu.dz (M. Berkani);
[*]cmdanesh@gmail.com (C. Danesh)

Abstract

Indole-3-acetic acid (IAA) represents a crucial phytohormone regulating specific tropic responses in plants, and functions as a chemical signal between plant hosts and their symbionts. The Actinobacteria strain of AW22 with high IAA production ability was isolated in Algeria for the first time and was characterized as *Streptomyces rubrogriseus* through chemotaxonomic analysis and 16S rDNA sequence alignment. The suitable medium for a maximum IAA yield was engineered *in vitro* and *in silico* using machine learning-assisted modeling. The primary low-cost feedstocks consisted of various concentrations of spent coffee grounds (SCGs) and carob bean grounds (CBGs) extracts. Further, we combined the Box-Behnken design from response surface methodology (BBD-RSM) with artificial neural networks (ANNs) coupled with the genetic algorithm (GA). The critical process parameters screened via Plackett-Burman design (PBD) served as BBD and ANN-GA inputs, with IAA yield as the output variable. Analysis of the putative IAA using thin-layer chromatography (TLC) and (HPLC) revealed RF values equal to 0.69 and a retention time of 3.711 min, equivalent to the authentic IAA. AW 22 achieved a maximum IAA yield of 188,290±0,38 µg/mL using the process parameters generated by the ANN-GA model, consisting of L-Trp, 0.6%; SCG, 30%; T°, 25,8°C; and pH, 9, after eight days of incubation. An R^2 of 99,98%, adding to an MSE of $1,86x10^{-5}$ at 129 epochs, postulated higher reliability of ANN-GA-approach in predicting responses, compared with BBD-RSM modeling exhibiting an R^2 of 76,28%. The validation experiments resulted in a 4,55-fold and 4,46-fold increase in IAA secretion, corresponding to ANN-GA and BBD-RSM models, respectively, confirming the validity of both models.

Keywords: Indole-3-acetic acid; *Streptomyces rubrogriseus*; Spent coffee grounds; Carob bean grounds; Model

1. Introduction

Indole-3-acetic acid (IAA), or Auxin, represents a crucial endogenous phytohormone modulating a variety of key plant physiological activities, starting from its role in shaping the plant morphology to the regulation of physiological growth activities (Grones et al., 2018; Qin et al., 2020; Rakusová et al., 2019). Indeed, IAA acts as a chemical signal coordinating the specific phenotypic responses of plants to environmental *stimuli*. These activities include cell-cell signalling, phototropism, gravitropism, *thigmotropism* (obstacle avoidance) and elicitation of plant defence (Gravel et al., 2007; Spaepen et al., 2007). Consequently, Auxin participates in abiotic stress alleviation (Huang et al., 2020; Zhou et al., 2020). Plants and microbes synthesize IAA via several interrelated pathways, including the tryptophan-dependent pathway (Duca and Glick, 2020). However, less information about auxin perception and signalling elucidates the accurate auxin-induced responses during plant growth (Gelová et al., 2021). Notably, multiple investigations revealed the capacity of *Streptomyces sp.* to synthesize physiologically active IAA to be oriented for industrial Auxin production (Boubekri et al., 2021; Myo et al., 2019). In recent investigations, economic carbon and nitrogen sources were employed as substitutes for expensive laboratory-grade medium components (Al Farraj et al., 2020; Bunsangiam et al., 2021; Lim et al., 2023).

Spent coffee grounds (SCGs) constitute a brewing process's derivate, are generally considered municipal solid waste, and contain around 75% of the original coffee bean (Wu et al., 2019). SCG are toxic pollutants rich in polyphenols, flavonoids, chlorogenic acid, and protocatechuic acid. These components have an essential antioxidant activity (Esquivel et al., 2012) and may disturb many life processes, adding to the massive oxygen quantity required for their decomposition (Hardgrove and Livesley, 2016; Lessa et al., 2018). Heat treatment, microbial degradation, and aerobic metabolism could considerably reduce SCG toxicity (Hao

et al., 2018). The total polysaccharides present in SCGs constitutes about 45.3% (w/w, dry weight) and are non-reducing sugars (Pasin et al., 2011).

Several factors such as nutritional and physiological parameters influence microbial growth and metabolic profile including auxin production. Optimizing tools help to study the significance and interaction of these parameters on the output during the bioprocess.

For this purpose, machine learning (ML) modelling methods may provide prospective substitutes for controlling or simulating targets using examples or experience (Schmidt et al., 2019). Nonetheless, the microbiological behaviour and metabolic processes are highly complex, less predictable and require a broad range of experiments susceptible to several physiological as well as nutritional process parameters (Medjili et al., 2023).

Modelling microbial growth and its metabolite production has recently been encouraged using empirical models, including response surface methodology (RSM) and artificial neural networks (ANNs). In media engineering, RSM constitutes a frequently exploited statistical approach for the generation of non-linear quadratic models and simultaneous bioprocesses factors optimization (Ribeiro et al., 2003; Roy et al., 2018). RSM integrates statistical and mathematical modelling into the experimental design and proceeds to treat complex data (Qin et al., 2012; Saini et al., 2020).

Artificial intelligence (AI) assisted methods like ANNs are adaptable process models with several interconnected units inspired by the brain's structure. ANN exhibits excellent accuracy in simulating and modelling complex and multivariate nonlinear targets (Desai et al., 2005). The phenomenon need not be mathematically described, and ANN can manage incomplete data from inputs and outputs (Aghaeinejad-Meybodi et al., 2019). Although ANN is an efficient tool to predict and optimize *in silico* complex process parameters with

universal approximation capability (Desai et al., 2008), it cannot guarantee the viability of the optimal global solution (Rajendra et al., 2009). These units are called artificial neurons (Vasseghian et al., 2021).

Genetic algorithm (GA) among other meta-heuristic optimization algorithms are founded on the principles of natural selection (Gherbawy et al., 2012; Jiang et al., 2014; Ousaadi et al., 2021; Poh et al., 2016). These algorithms do not easily get trapped in a local minimum (Agarwal et al., 2016; Ghaedi et al., 2015a, 2015b; Jiang et al., 2014; Zhang and Pan, 2014). GA relies on the Darwinian genetic evolution principle and uses genetic operators, including selection, mutation and/or inversion, and crossover, to identify the problem's optimal solution (Smaali et al., 2021; Yahya et al., 2020). This procedure is called the fitness function (Ghaedi and Vafaei, 2017). This operation is repeated several times over generations to generate the fittest chromosomes, constituting the solutions or the optimal operating variables for the studied bioprocess. Thus, GA represents a suitable evolutionary, adaptive optimizer often coupled with ANN and finds the precise or approximate optimal operational parameters for a single exclusive target, such as IAA production, with satisfying performance while reducing ANN complexity (Fan et al., 2018).

Our primary motive resides in formulating an appropriate low-cost medium composition to achieve maximum IAA output using SCG as a feedstock substrate. This approach relies upon combining RSM with ANN-GA to determine the proper optimization of the low-cost, nutritionally adequate process parameters in submerged fermentation. The two models' predictive performance and modelling efficiencies were assessed according to the correlation coefficient (R2) with the absolute error. Variance (ANOVA) and Sensitivity analysis were conducted to examine the relative significance of inputs.

In the present study, the experimental design of Plackett-Burman (PBD) was conducted to effectively categorize the most significant process parameters impacting the fermentation process. Subsequently, determining the approximate range of the pre-identified key factors using Box-Behnken design (BBD) and establishing the regression model to measure Auxin content in a low-cost medium (Zhao et al., 2013). Finally, optimal fermentation conditions for the low-cost bioprocess for IAA production from *Streptomyces sp.* were optimized using ANN-GA. It is the first report on the effective valorization of SCG or CBP as media components for producing actinobacteria-originated IAA. This research sheds important light on the critical operating conditions affecting the bioprocess for the semi-pilot or large-scale synthesis of agroactive compounds, including IAA, for further sustainable use in agriculture.

2. Materials and methods

2.1. Isolation of *Streptomyces*-Like isolates

Actinobacteria were isolated from a semi-arid, nonsaline rhizospheric soil, collected from different wheat-growing fields in the Tiffeche Region (36° 9' 24" N; 7° 41' 56" E) of Souk-Ahras Province in Algeria. Further, incubation on Starch Casein Agar agar (Starch 10 g/L, Casein 1 g/L, K_2HPO_4 0.5 g/L, Agar 13 g/L, pH 7.2) was carried out for 7-14 days at 28°C, as earlier suggested by (Kusuma et al., 2020). After detaching the healthy wheat roots from the soil with no visible damage, the bulk soil was withdrawn by shaking the roots. The soil that was still firmly adhered was recovered as rhizospheric soil, and it was safely transferred and stored at 4°C until use. Then, 1 g of $CaCO_3$ was incorporated into 4-5 g of soil samples. The samples were further dried for one hour at 45°C (Suárez-Moreno et al., 2019). 28 Streptomyces-like strains were isolated according to their microscopic and macroscopic

features and subsequently characterized on International Streptomyces Project media (ISP2, ISP3, and ISP4) (van der Aart et al., 2019; Yan et al., 2018). The catalase and oxidase tests and carbon source utilization were assessed, as indicated for *Streptomyces*-like bacteria (Shirling and Gottlieb, 1968). Mycelial fragments and spores of pure colonies were sustained in 15%, v/v glycerol at -20°C and -80°C (Shirling and Gottlieb, 1966).

2.2. Screening for IAA production

The aptitude of actinobacteria strains to synthesize and release IAA was assessed according to Khamna et al. (2010). One millilitre aliquot of *Streptomyces*-like spore suspensions (~ 10^6 spores ml^{-1}) was introduced into 250 mL Erlenmeyer flasks comprising 100 ml of yeast extract-tryptone broth (YTB) amended with 0.2% (w/v) L-tryptophan then incubated for eight days at 30 °C under the agitation of 150 rpm.

2.3. Auxin assay

Cultures' supernatants were recovered via filtration through Whatman filter paper n°1, followed by centrifugation (20 min at 4000×g) on the eighth day of incubation. The absorbance of the samples was measured at 530 nm using a Helios epsilon UV-vis spectrophotometer (Germany), and IAA concentration was estimated according to a standard curve prepared with an authentic IAA purchased from Sigma, USA (Passari et al., 2015). The IAA concentration was investigated by colourimetric assay (Bano and Musarrat, 2003) by mixing the culture supernatant with the Salkowski reagent at a ratio of (1:2), respectively (Sadeghi et al., 2012). A developed pink-red colour after 30 min of incubation in the darkness indicates indole compound production by actinobacteria.

197 **2.4. Enzyme production and physiological characteristics**

198 **2.4.1. Protease Production**

199 Actinobacteria isolates were spot inoculated on 10% (v/v) skimmed milk agar (SMA) to
200 detect extracellular proteases. SMA consists of a stock solution of skimmed milk and agar
201 solution autoclaved individually at 115°C for 10 minutes and 121°C for 20 minutes,
202 respectively. The two solutions were mixed at 60°C to a 1% final concentration of skimmed
203 milk. After incubation at 30°C for 48–72 hours, the formation of clear zones around the
204 colonies indicated extracellular caseinase production (Abdelmoteleb et al., 2017).

205 **2.4.2. Cellulase Production (cellulolytic activity)**

206 The cellulolytic activity, the cleavage of amorphous cellulose, was assessed semi-
207 quantitatively on the minimal medium agar amended with 1% (w/v) Carboxymethyl
208 cellulose (CMC) as the sole energy and carbon source [in g/l: $NaNO_3$, 1.2; K_2HPO_4, 6;
209 KH_2PO_4, 3; $MgSO_47H_2O$, 0.2; $CaCl_2$, 0.05; $MnSO_47H_2O$, 0.01; Zn SO_47H_2O, 0.001; Agar, 15; pH
210 7.0]. CMC plates were spot inoculated with 5-day-old cultures in the petri dish centre, then
211 incubated for five days at 30°C (Ahirwar et al., 2017). The CMC degradation ability of the
212 strain was detected after flooding plates with 0.1% Red Congo (aqueous) solution for 30
213 minutes, then destained using 1 M NaCl solution to make the hydrolyzed zone visible and
214 clear. Cellulase activity was revealed by the colonies developing a visible halo (Slama et al.,
215 2019; Suárez-Moreno et al., 2019).

216 **2.4.3. Lignin oxidation activity**

217 The ability of the strain to develop on purified lignin was evaluated on the minimal medium
218 containing 0.5% (w/v) craft Lignin as the sole carbon source [in g/l: $NaNO_3$, 1.2; K_2HPO_4, 6;
219 KH_2PO_4, 3; $MgSO_47H_2O$, 0.2; $CaCl_2$, 0.05; $MnSO_47H_2O$, 0.01; Zn SO_47H_2O, 0.001; Agar, 15; pH

7.0]. The colony growth after incubation at 30°C for five to seven days indicates a positive result.

2.4.4. Amylase production

Spot inoculation of the actinobacteria isolate on Starch-Casein Agar media containing 1% (w/v) of soluble starch was performed [in g/l: Starch, 10; Casein, 0.3; KNO_3, 2; $MgSO_47H2O$, 0.05; K_2HPO_4, 2; NaCl, 2; $CaCO_3$, 0.02; $FeSO_47H_2O$, 0.01; Agar, 15; pH 7.0]. This Method enables the assessment of starch hydrolyzation mediated by Amylase activity. After incubation for three to four days at 30°C, Lugol's iodine solution [in (w/v) iodine, 5% and KI/L, 10%) was poured on the plates' surface. Prominent halo development around the colonies is an indicator of a positive amylolytic activity of the isolated (Slama et al., 2019).

2.4.5. Chitinase production

The chitinolytic activity of *Streptomyces*-like strain was detected according to Gonzalez-Franco et al. (2003). The isolate (10µL of five-day-old cultures, 10^6 spore/mL) were spot inoculated on colloidal chitin agar medium (0.4%) (w/v) then incubated for five to seven days at 30 °C. The colloidal chitin agar media (pH 7.0± 0.2) consisted of [in (g/L): (K_2HPO_4, 0.7; KH_2PO_4, 0.3; $MgSO_4$ X5H_2O, 0.5; $FeSO_4$ X 7H_20, 0.01; $ZnSO_4$, 0.001; $MnCl_2$, 0.001; agar, 15), supplemented with 0.4% moist colloidal chitin as the sole carbon supplier (Gómez Ramírez et al., 2004; Murthy and Bleakley, 2012). A halo surrounding the colonies revealed the chitinolytic activity of the test strain (Murthy and Bleakley, 2012; Zamoum et al., 2015).

2.4.6. Plant sugar utilization profile of AW22

Determination of sugar utilization profile of selected isolate was adapted to a 96-well microplate using Minimal medium (MM) [in g/l: $NaNO_3$, 1.2 ; K_2HPO_4, 6 ; KH_2PO_4, 3 ; $MgSO_47H_2O$, 0.2 ; $CaCl_2$, 0.05 ; $MnSO_47H_2O$, 0.01 ; Zn SO_47H_2O, 0.001 ; pH 7.0±0.2] amended

243 with 0.2% (w/v) of Fructose, Mannose, Maltose, Xylose, Arabinose, Lactose, Galactose,
244 Sucrose, Mannitol, Ribose and Rhamnose. Phenol red (PR) was used as a pH indicator
245 instead of Bromocresol purple (BCP). All sugars were filter-sterilized into the MM after
246 autoclaving. The positive control consisted of MM supplemented with 0.2% (w/v) glucose,
247 while MM devoid of any added carbon source was employed as a negative control. 96 well
248 Microplates were UV-sterilized for 20min before utilization. Each well was filled with 180µl
249 MM (with and without C source) completed to a volume of 200µl with spore suspension (10^6
250 spore/ml). The assay was performed in triplicates. For five days, parafilm-sealed microplates
251 were incubated at 28°C under slow agitation (100 rpm) and examined periodically. The
252 colour change of the PR into yellow indicated a positive result.

253 **2.4.7. Nitrogen source utilization profile**

254 The utilization of amino acids as the sole nitrogen source by the selected actinobacteria strain
255 was also evaluated (Williams et al., 1983). Each nitrogen source (proline, glycine, leucine, and
256 L-asparagine) was introduced to the basal medium (pH of 7.0±0.2) at final concentration of
257 0.1% (w/v) and incubated for 14 to 21 days at 30°C at.

258 **2.4.8. Physiological characterisation**

259 The physiological characteristics of actinobacteria isolate to grow at different temperatures
260 (4, 15, 20, 25, 30, 35, 40 and 45°C), at different pH (5.0, 7.0 13.0 ±0.2 pH unit) and to tolerate
261 Phenol 0.5%, Tellurite 0.5%, Sodium azide 0.1% and NaCl concentration from 0–10% (w/v) at
262 1.0 NaCl unit intervals) were examined. These characteristics were evaluated on GYM agar
263 after 14 days of incubation.

264 AW 22 growth was recorded according to the following scale: -: no growth, +: weak growth,
265 ++: moderate growth, +++: abundant growth.

2.5. Molecular identification of the higher IAA producer actinobacterium

16S rRNA gene sequencing was used to identify strain AW 22 taxonomically. PCR was carried out using the universal primers 27F (5′-GAGTTTGATCCTGGCTCAG-3′) and 1492R (5′ TACGGYTACCTTGTTACGACTT-3′) according to the protocol outlined by Girão et al. (2019). Genomic DNA extraction, 16S rRNA gene amplification by PCR, and sequencing of purified PCR products were performed in ALVALAB, Spain. Using the NCBI BLAST database for Bacteria and Archaea, the 16S rDNA sequences were examined, and the phylogenetic affiliation of the isolate was determined. This affiliation was then validated using the identification tool from EzTaxon and the sequence match tool from the Ribosomal Database Project. Further, the phylogenetic tree was developed to support the taxonomic analysis of the isolates. In compliance with the BLAST results, the nearest neighbours sequences in GenBank were chosen, and MUSCLE was used to align each sequence fulfilling these requirements. Next, the Tamura-Nei model-based Neighbour-joining method was used to create the phylogenic tree using 1000 bootstraps. The MEGA11 program, which stands for Molecular Evolutionary Genetics Analysis, was used to perform the evolutionary analyses (Tamura et al., 2021).

2.6. Time course of IAA and biomass production from strain AW 22

The appropriate incubation time for IAA and biomass yield by AW 22 was evaluated at 24 h intervals for ten days on GYM broth supplemented with L-Tryptophan at 0.2% (w/v). The development of biomass was measured using the traditional oven method (Buono and Erickson, 1985). Briefly, AW 22 cultures were filtered via Whatman filter paper (No. 1) and dried at 70 °C for 12h to estimate dry biomass weight. All experiments were performed with an inoculum size of 3.8×10^{6} CFU/mL of AW 22 cells and conducted in triplicate to obtain average values.

290 **2.7. Extraction and TLC confirmation of IAA**

291 The synthesis of IAA was verified by thin-layer chromatography (TLC), as reported by
292 Goudjal et al. (2013). Extracts were separated with Ethyl Acetate (EA) at a ratio of (1:3) (v/v)
293 and vacuum evaporated at 40°C.

294 EA fractions of 10–20 µl were spot-deposited on TLC plates (silica gel GF254, thickness 0.25
295 mm, Merck, Germany) and processed in ethyl acetate: chloroform: formic acid (55:35:10, by
296 volume). TLC plates were treated with Ehmann's reagent before their visualization under
297 UV light (254 nm), displaying spots with identical Rf values to the standard IAA.

298 **2.8. High-Performance Liquid Chromatography (HPLC) for IAA quantification**

299 EA fractions were subjected to an HPLC (Agilent Technologies, USA) equipped with a UV
300 detector and a column model Cosmosil SC18-MS-II (Nacalai Tesque, Japan). The elution
301 system and the flow rate were optimized and adapted from (Bunsangiam et al., 2021; Kaur &
302 Kaur, 2021; Myo et al., 2019; Nutaratat et al., 2015). The mobile phase's solvent system
303 consisted of acetonitrile: water: acetic acid (35:65:1 v/v/v) at a 1 mL/min flow rate (Nakurte et
304 al., 2012) with a 20 µL injection volume. Thus, the isocratic elution method was preferred
305 over gradient elution while the column temperature was sustained at 25°C. As the standard,
306 authentic IAA (Sigma, USA) was used to quantify IAA in the sample. IAA detection was
307 monitored at 280 nm.

308 **2.9. SCG and CBP extract preparation**

309 SCG extract was prepared according to the hydrothermal method adapted from (Rajendran
310 et al., 1991). Samples of SCG were collected from coffee shop consumption of Robusta coffee
311 beans at 85°C, Algeria. Carob extracts were obtained from freshly collected carob beans.

Substrates were either air-dried for fifteen days or heat-dried for eight hours at 60°C for, and Carob beans were chopped, ground and sieved.

Briefly, 200 grams of dried SCG/ CBP were mixed with 1000 mL of deionized water were autoclaved at 121°C for one hour, and samples were cooled to room temperature overnight, then stocked at 4°C. Subsequently, samples were extracted by filtration through cheesecloth and Whatman No. 1 filter paper to obtain SCG and CBP extract solution (Wu et al., 2019).

2.10. Influence of carbon source concentrations on IAA yield

The influence of substrate concentration on the ability of strain AW 22 to produce IAA was assessed. Briefly, minimal medium was amended with Glucose at 0.2%, 0.5% and 1% (v/v), Carob Beans Powder extract at 10-50% (v/v), SCG extract medium at 10-50% (v/v) and L-Trp at 0.2% (w/v). The minimal medium devoid of L-Trp consisted of negative control while the Glucose 0.5% consisted of positive control. AW 22 cultures were inoculated and incubated at 28 °C for 8 days under permanent shaking at 150 rpm.

2.11. Plackett-Burman design (PBD) screening of significant parameters

This approach aims to select the most influential media components (Khosravi-Darani and Zoghi, 2008; Purama and Goyal, 2008) on IAA production. After determining the maximum IAA yield according to the time course experiment, the experimental design of Plackett-Burman was employed for the screening of fourteen independent variables. These parameters consist of eleven nutrient factors (L-Tryptophan, SCGE, CBPE, $CaCO_3$, Yeast extract, soluble starch, Tryptone, NaCl, K_2HPO_4, $MgSO_4$) (Zhao et al., 2013), three culture conditions (pH, growth temperature, incubation time) and Inoculum amount (in %) (v /v).

All independent factors were assessed at two widely-spaced intervals, represented as negative values (low level, − 1) and positive values (high level, + 1) in 20 experiments. Each row represents a trial with a response value consisting of IAA yield.

336 The factors' actual levels are listed in Table 1, while the BBD matrix in coded units is
337 summarized in Table 2.
338 All experiments were performed in triplicate, and the mean value constituted the response.
339 The statistical metrics of the model were determined via the analysis of variance (ANOVA).
340 The variables' significance was estimated by calculating the *p*-value and confidence levels
341 using the standard regression analysis. Factors presenting a 5% level of significance ($p<0.05$)
342 were further optimized with BBD to increase IAA yield. The PBD first order model is given
343 in equation (1):

344 $$Y = \beta_0 + \sum \beta_i x_i \qquad \text{Eq. (1)}$$

345 where Y stands for the dependent variable (response = IAA production), β_0 corresponds to
346 the model' intercept, β_i represents the regression coefficient, and x_i is the independent
347 variable. Minitab 19.0 statistical software package was used for the PBD and results analysis.
348
349 **Table 1**. Actual values of independent variables screened by PBD.

Facto label	**Variables**	**Unit**	**level**	
			-1	**1**
X1	CBP	%	30	50
X2	SCG	%	30	50
X3	Starch	g/L	2	5
X4	Tryptone	g/L	3	6
X5	Yeast E	g/L	2,5	5
X6	L-Trp	%	0,3	0,6
X7	NaCl	g/L	1	5
X8	K2HPO4	g/L	0,3	0,7
X9	MgSO4	g/L	0,2	0,5

X10	CaCO3	g/L	1,0	1,5
X11	Incub. Time	Day	6	10
X12	T	°C	26	35
X13	pH	-	7±0,1	9±0,1
X14	Inoc. amount	%	2	4

350 Note: X_1-X_{14} correspond to various impact variables; "1" and "-1" are two different levels.

351

352 **Table 2**. Plackett–Burman experimental design matrix represented in coded units.

Run N°	X1	X2	X3	X4	X5	X6	X7	X8	X9	X10	X11	X12	X13	X14
1	+	-	+	+	+	+	-	-	+	+	-	+	+	-
2	-	+	-	+	+	+	+	-	-	+	+	-	+	+
3	+	-	+	+	-	-	-	-	+	-	+	-	+	+
4	-	-	-	-	-	-	-	-	-	-	-	-	-	-
5	+	+	-	-	-	-	+	-	+	-	+	+	+	+
6	+	-	-	-	-	+	-	+	-	+	+	+	+	-
7	+	-	+	-	+	+	+	+	-	-	+	+	-	+
8	+	+	-	+	+	-	-	-	-	+	-	+	-	+
9	+	-	-	+	+	-	+	+	-	-	-	-	+	-
10	-	+	-	+	-	+	+	+	+	-	-	+	+	-
11	-	+	+	-	-	-	-	+	-	+	-	+	+	+
12	-	-	-	-	+	-	+	-	+	+	+	+	-	-
13	-	-	+	+	-	+	+	-	-	-	-	+	-	+
14	+	+	+	+	-	-	+	+	-	+	+	-	-	-
15	-	+	+	-	+	+	-	-	-	-	+	-	+	-
16	-	+	+	+	+	-	-	+	+	-	+	+	-	-
17	-	-	-	+	-	+	-	+	+	+	+	-	-	+
18	+	+	-	-	+	+	-	+	+	-	-	-	-	+
19	-	-	+	-	+	-	+	+	+	+	-	-	+	+
20	+	+	+	-	-	+	+	-	+	+	-	-	-	-

353 Note: X1 ~ X14 represent the impact variables; "1" and "-1" correspond to two different levels; 1 to 20
354 represent 20 different sets of fermentation conditions.

355 **2.12. Box-Behnken design (BBD) of Response surface methodology (RSM)**

356 The four highly significant process parameters obtained from PBD (SCG, L- tryptophan
357 concentration, incubation temperature and pH) were later subjected to RSM analysis using
358 the Box-Behnken design (Lanka and Latha, 2015). Minitab 19.0 statistical software package
359 optimised response and correlating the independent variables mathematically(Ousaadi et al.,
360 2021).

361 This study generated twenty-eight experiments for 4-factor BBD with four central points. All
362 factors were evaluated at three levels (+ 1, 0 and − 1), where 0 corresponds to the coded
363 central value, + 1 is a high value, and − 1 is a low value to optimize the key factors (Actual
364 and coded values are given in table 3 and 4, respectively).

365 All experiments were conducted in triplicate, and the calculated average IAA concentration
366 served as the experimental response value. Further, all responses were fitted to an
367 independent second-order polynomial model represented in equation (2):

368

369 $$Y = \beta_0 + \sum \beta_i x_i + \sum \beta_{ii} x_i x_j + \sum \beta_{ij} x_i x_j \qquad \text{Eq. (2)}$$

370

371 Where:

372 Y stands for the predicted value of the output variable (IAA production).

373 β_0 constant term coefficient (the intercept).

374 β_i, β_j and β_{ij} are the linear, quadratic, and interaction term coefficients, respectively.

375 x_i and x_j are the coded independent variable.

376

The correlation between xi coded value for X_i, which represents the independent variable's actual value and is expressed as follows (Eq. 3):

$$x_i = \frac{X_i - X_0}{\delta X} \qquad \text{(Eq.3)}$$

X_0 denotes the independent variable's actual value at the central test point, and the step change in X_i is represented by δX.

i=1,2,3…

The regression equation also served to calculate predicted response values. A variance analysis (ANOVA) resolved the model's statistical competence. F- and *p*-values evaluate the factors' significance and the regression model. Thus, a great Student's *t*-test with a low *P*-value testifies to the high reliability of the regression model (Vasseghian et al., 2020).

The coefficient of determination (R^2) with the adjusted R^2 was used to statistically evaluate the accuracy and assess the reliability of the polynomial model equation.

Developing contour plots help to elucidate the correlations between the responses and the experimental levels of every independent variable. Subsequently, the software's response optimizer tool served to designate the best value for each variable to achieve the highest IAA yield.

2.13. Experimental validation of the fitted model

The fitted model was experimentally validated, and strain AW 22 was inoculated on the optimal medium according to the combination of different optimized variables (culture conditions) suggested by BBD. The culture conditions and the target response are recorded

399 in Table 12. The *in silico* optimization predicted the maximum IAA response with desirability

400 1.

401 **Table 3**. Actual and coded values for the independent variables evaluated in the BBD.

Level	Factors			
	L-Trp (%)	SCG (%)	Temperature (°C)	pH
-1	0,2	30	26	7,1
0	0,4	40	30	8,05
1	0,6	50	35	9

402

403 **Table 4**. Experimental matrix of Box Behnken Design in coded units including experimental

404 data.

Run	Variables				IAA yield (μg/mL)		
	A	B	C	*D*	*Y* (Test value)	*Y* (Fit value)	Residual
1	1	0	1	0	173,06±6,23	179,99	-6,93
2	0	0	0	0	177,18±6,34	120,29	56,88
3	0	1	1	0	86,28±2,74	102,29	-16,01
4	0	1	0	1	74,11±4,63	82,33	-8,22
5	1	0	-1	0	64,20±1,82	98,62	-34,41
6	0	1	-1	0	80,87±3,57	54,46	26,41
7	-1	0	1	0	77,37±10,03	46,89	30,48
8	-1	0	-1	0	34,36±1,54	31,37	3,00
9	0	0	0	0	76,99±4,96	120,29	-43,31
10	-1	0	0	1	31,20±1,37	50,43	-19,22
11	-1	1	0	0	18,56±1,26	22,21	-3,66
12	1	0	0	-1	184,36±7,85	184,02	0,35
13	0	0	1	-1	159,27±6,94	138,15	21,12
14	1	1	0	0	115,35±7,31	92,36	22,99
15	0	-1	0	1	94,23±4,82	76,65	17,58

16	0	0	0	0	155,68±9,42	120,29	35,38
17	-1	0	0	-1	25,31±2,88	35,73	-10,42
18	1	-1	0	0	176,60±7,12	150,14	26,47
19	0	-1	-1	0	78,71±5,71	81,58	-2,87
20	0	-1	1	0	85,37±1,96	130,66	-45,29
21	0	0	-1	-1	129,96±2,80	123,77	6,19
22	0	0	0	0	71,34±5,05	120,29	-48,96
23	0	0	-1	1	57,97±6,20	56,28	1,69
24	0	1	0	-1	60,80±9,14	82,32	-21,52
25	0	0	1	1	155,44±9,00	138,81	16,63
26	-1	-1	0	0	19,76±2,61	19,93	-0,18
27	1	0	0	1	94,04±3,59	102,49	-8,46
28	0	-1	0	-1	147,77±12,37	143,49	4,28

405

406 **2.14. Machine learning assisted optimization of IAA production**

407 The input, hidden, and output layers, are the distinct divisions of the several neurons that
408 constitute an ANN. The operating units acting as feature detectors and introducing
409 nonlinearity into the network are the hidden layers, which can be single or multi-architecture
410 (López et al., 2017). The elaboration of an ANN model depends on several phases. The
411 training phase (*Input feed-forward multilayer* and error backpropagation) and the validation
412 phase. The feed-forward back propagation (BP) or Levenberg-Marquardt (trainlm) algorithm
413 was adopted to create and train an ANN model using the BBD data that was previously
414 presented. However, as proposed by (Maji et al., 2014), data points were increased up to 200
415 and generated based on the second-order polynomial equation, as the experimental data sets
416 from BBD were insufficient for creating an optimal network architecture. The validation
417 procedure aimed to reset the reliability of the built-in model during the training phase. The

418 model can be used in subsequent applications only when the validation results match
419 expectations.

420 **2.14.1. Artificial neural network modeling**

421 The typical input feed-forward multilayer ANN (MLP) was combined with a training
422 algorithm for ANN modeling at this level. MLPs are straightforward universal
423 approximators and are frequently considered for modeling physicochemical processes
424 (Jasso-Salcedo et al., 2017; Moghri et al., 2017).

425 Three subdivisions of the datasets were generated. Each subset contained 70% of the data for
426 testing, 15% for validating, and 15% for network training. Inputs and outputs represent fixed
427 components in the ANN topology (architecture). At the same time, the hidden layers'
428 number and their respective neurons constitute a series of variable elements. Typically, bias
429 and weights express the connections between each layer. Aside from network topology,
430 internal parameters are selected according to the empirical data to achieve the best ANN
431 identification.

432 Therefore, around 11 alternative training algorithms and a five-fold cross-validation strategy
433 were applied to identify the ANN core parameters and the appropriate amount of hidden
434 neurons.

435 The system's inputs for the current process are the initial concentrations of L-Trp
436 concentration (X1), operating temperature (X2), initial pH (X3), and SCG concentration (X4),
437 while the system's output is the yield of IAA. Two hidden layers were chosen, consisting of a
438 neuron number between [1-10] intervals.

439 Figure 1 shows the current ANN simple structure, and Table 5 **s**ummarizes the design
440 parameters adopted in developing the present ANN model.

441 **Table 5**. Parameters adopted in creating the ANN model.

Type	Description
Inputs layer	4 neurons (L-Trp concentration, SCG concentration, T°, pH)
Hidden layer	n= 2 layers; m= 12 neurons
Output layer	1 neuron (IAA yield)
Learning rate	0.01
Epoch	1000
MSE goal	0.001
Algorithms	Levenberg-Marquardt (trainlm)
Function	Sigmoid (tansig): preferred between input and hidden layers
	Linear: preferred between hidden and output layers

442

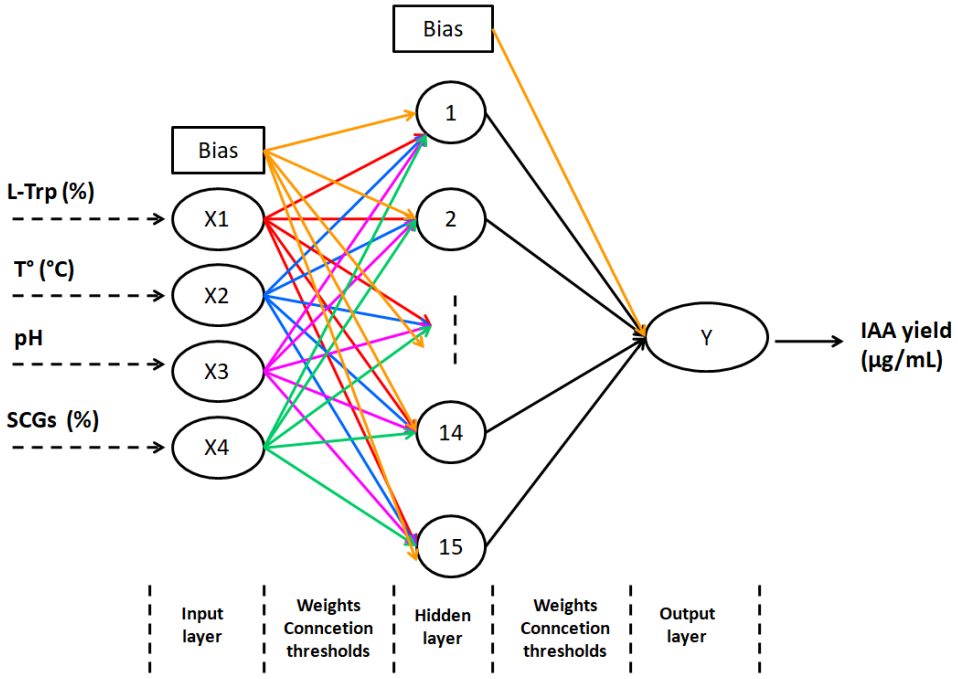

443

444 **Fig. 1**. Typical design of the current artificial neural network (ANN).

445

446 A three-layered BP-ANN was elaborated in this study. An activation function is first
447 executed to generate a simulated output on a network that has been trained with random

weights and bias values. The activation functions convert the weighted sum of the input to generate the output (Çelekli et al., 2013).

The hidden layer-emitted signals are expressed in weights, and thresholds through transferring function, as described in equation (4). Still, the hidden-to-output layer-oriented signals constitute the predicted value that may be expressed by the equation (5).

$$x_j = F\left(\sum_{i=1}^{n} x_i \times w_{ij} + P_j\right) \qquad \text{Eq. (4)}$$

$$y_{i-pred} = F'\left(\sum_{i=1}^{n} v_j \times x_j + Q\right) \qquad \text{Eq. (5)}$$

where:

xi, bj represent the input and the hidden neuron values, respectively.

wij and *vj* correspond, respectively, to the weights between *xi* (input neuron) and *xj* (hidden neuron) and *xj* (hidden neuron) and the output neuron.

Pj and *Q* represent the connection thresholds of the hidden and output neurons, respectively.

F means the transfer function between *xi* and *xj*; *F'* means the transfer function between *xj* and the output neurons.

$Y_{i\text{-}pred}$ is the IAA concentration predicted value.

wij, *Pj*, *vj*, and *Q* are first arbitrarily designated low values for subsequent readjustments during the feedback process.

The output and hidden layers have *linear* and *tangent sigmoid* transfer functions, respectively.

All the ANN model's training values were normalized between 0 and 1 via the min-max method expressed in equation (6) to prevent numerical overflows brought on by larger or smaller weights:

$$x_i = \frac{X_i - X_{min}}{X_{max} - X_{min}} \qquad \text{Eq. (6)}$$

where X_i, X_{min} and X_{max} represent the normalized, least and highest values of X (original value), respectively.

After training, the BP algorithm is processed with the *error backwards propagation* to diminish the prediction mean squared error (MSE) iteratively between experimental and simulated output data and continuously adjust weights and biases between the neurons.

As performance indices, the MSE Eq. (7) and the determination coefficient (R^2) (Eq. 8) served to create an ideal ANN model capable of assessing the predictions accuracy made between the ANN outputs and the targets (Dhanarajan et al., 2014; Sivapathasekaran et al., 2010; Vasseghian and Dragoi, 2018). Based on the minimum value of MSE, the hidden neurons' amount was designated (Rajendra et al., 2009). Subsequently, an optimal network topology was selected depending on the least MSE and maximal R-values to prevent data over-fitting and enhance the accuracy and predictability of outputs (Dhanarajan et al., 2014; Huang et al., 2007).

$$MSE = \sum_{i=1}^{n} \frac{(y_i - y_{i-pred})^2}{n} \qquad \text{Eq. (7)}$$

$$R^2 = \frac{\sum_{i=1}^{n} (y_i - y_{i-pred})^2}{\sum_{i=0}^{n} (y_{i-av} - y_{i-pred})^2} \qquad \text{Eq. (8)}$$

where $y_{i\text{-}pred}$ and y_i correspond to the predicted and provided output values, respectively, and n is the respective number of provided data points for the corresponding phase (training, testing, or validation), $y_{i\text{-}av}$ is the average value.

The hidden neuron weight (*Wj)* can be computed according to equation (9), which can be put forward:

$$W_j = \sum_{i=1}^{k} w_{ij} x_i \qquad \text{Eq. (9)}$$

where k represents the input layer-related number of neurons, w_{ij} is the connection weight between x (output neuron) and b (hidden neuron).

i is the input layer neuron, and x_i represents its value.

Similarly, the output neuron weight (*Wk)* can be computed according to equation (10):

$$W_k = \sum_{j=1}^{z} w_{jk} x_j \qquad \text{Eq. (10)}$$

where z represents the hidden layer-related number of neurons, w_{jk} is the connection weight between j (hidden neuron) and k (output neuron).

j is the hidden layer neuron, and x_j represents its value.

The activation function generates the predicted output using the neuron's weight in the hidden or output layer according to equation (11).

$$y = f(W + B) \qquad \text{Eq. (11)}$$

where:

y stands for the predicted output.

f is the activation function.

W and B represent the weight and bias in the hidden or output layer.

514 The cross-validation procedure was performed ten times to improve predictability and
515 accuracy, with the results averaged.

516 **2.14.2. Sensitivity analysis**

517 The connection weights were investigated, and the input factors' relative influence on the
518 output was evaluated through the Garson algorithm's sensitivity analysis (Zhang and Pan,
519 2014). For this kind of analysis, the Garson equation (Eq. 12) and potential combinations of
520 variables were used (Aleboyeh et al., 2008; Yetilmezsoy and Demirel, 2008).

521 $$Q_{ik} = \frac{\sum_{j=1}^{L}\left(\frac{|w_{ij}|}{\sum_{r=1}^{N}|w_{rj}|}|v_{jk}|\right)}{\sum_{i=1}^{N}\left(\sum_{j=1}^{L}\left(\frac{|w_{ij}|}{\sum_{r=1}^{N}|w_{rj}|}|v_{jk}|\right)\right)} \qquad \text{Eq. (12)}$$

522 The Q_{ik} stands for the impact percentage of the input variable. The connection weight
523 between i and j, the input and the hidden neuron, respectively, is indicated by w_{ij}.
524 The connection weight between j and k the hidden and the output neuron, respectively, is
525 represented by v_{jk}, and the connection weight between the input neuron N and the hidden
526 neuron j is defined by w_{rj}.
527 N, L, and M are the neurons' numbers in the input, hidden, and output layers.
528 w and v are the connection weights between the input and the hidden layers and between the
529 hidden and the output layers.

530 **2.14.3. Genetic algorithm-assisted optimization**

531 The genetic algorithm constitutes an AI-based stochastic nonlinear optimization formalism
532 that simulates natural selection and genetic mechanisms (Jiang et al., 2014). GA prevents the
533 models from being trapped by local optima by selecting suitable initial weights and

thresholds for the previously generated ANN model and utilized as a fitness function (Eq. 13). The fitness function can be expressed as follows:

$$F = Purelin\left(JW * \tan sig\left(KW * [x_1; x_2; x_3; x_4] + b_j\right) + b_k\right) \quad \text{(Eq. 13)}$$

Where F denotes the IAA yield, b_k and JW stand for the output layer's bias and weight, and b_j and KW represent the hidden layer's bias and weight, respectively.

The IAA production bioprocess optimization using the GA algorithm followed several steps: initialization, selection, crossover, and mutation with different parameters and, relying on particular characteristics, using various rules.

The default "ga" function in MATLAB interprets and treats the elementary data of the parameters requiring optimization, such as the initial weights and thresholds as chromosomes. The higher fitted chromosomes will be chosen by means of genetic reproduction, including crossover and mutation, while the least fitted ones will be substituted (Jiang et al., 2014). GA is reportedly adept at global searching to achieve convergence, independent of the initial value.

(1) GA starts by providing an initial population of solutions or individuals using initial operating temperature, pH, and L-Trp and SCG concentrations as optimization inputs. The ANN model-related initial weight and threshold were obtained and encoded into binary strings forming the chromosomes.

(2) Subsequent selection of outstanding chromosomes with high fitness from the present population is based on the coefficient of fitness for every chromosome. This operation helps to propagate excellent offspring and eliminates the low fitness chromosomes (Jiang et al., 2014).

(3) The remaining chromosomes are treated using evolutionary operators crossover and mutation to improve the offspring of parents and produce the next generation (Yetilmezsoy and Demirel, 2008). Crossover aims to exchange data and genes among individuals, whereas mutation randomly affects individuals from the population and alters their genes (Bagheri et al., 2015).

(4) The fitness function (step 2) is carried out iteratively until the chromosomes have attained the maximum fitness level, and the convergence forms the optimal solution.

(5) The last step entails decoding all chromosomes and substituting the ANN model's starting weights and threshold with these upgraded ones.

For this work's purpose, the settings taken into account are summarized in table 6. Nonetheless, the selection function output is multiplied by-1 since the GA algorithm aims to minimize and not maximize outcomes.

Table 6. GA configuration for the IAA production model implementation.

Parameters	Value
Population size	200
Number of elite	2
Crossing fraction	1
Migration fraction	0.2000
Migration interval	20
Direction of migration	forward
Stall generation limit	20
Stall time limit	20
Plot Interval	1
Generations	100

570 ## 3. Results and discussion

571 ### 3.1. *Streptomyces*-like isolates and IAA production

572 Streptomyces represents the dominant genus of actinobacteria in soil ecosystems (Thakur et
573 al. 2007). This genus' members are typically isolated from plant tissues and the rhizosphere,
574 indicating their highly compatible nature with various host organisms and contributing to
575 improving their growth (Goudjal et al., 2014; Verma et al., 2009). Twenty-eight
576 morphologically distinct rhizospheric actinobacteria colonies were gram-positive
577 filamentous rods exhibiting *Streptomyces* aspects. Wrinkled and coloured colonies with waxy,
578 powdery, or velvety surfaces were among the traits (data not shown), which were obtained
579 from wheat rhizospheric soil samples from Tiffech province of Souk-Ahras, Algeria, upon
580 enrichment with $CaCO_3$. Our findings confirmed that the presence and distribution of
581 *Streptomyces*-like isolates in this newly explored province are slightly different, from a
582 metabolic point of view, from other reported niches, such as the river sand ecosystem. Thus,
583 previous studies correlated that the habitat affected actinobacteria diversity in the soil more
584 than the microbial communities (Abbasi et al., 2019). Interestingly, some nutrient restrictions
585 in the belowground constitute a significant factor in the diversity dynamics of soil
586 microbiomes because of natural selection.

587 In our study, primary screening consisting of a quantitative assessment of IAA synthesis by
588 *Streptomyces*-like strains found that all the wheat-associated isolates (100%) possess the
589 ability to yield IAA (Fig. 2) ranging between 1,8534± 0,1724-23,999±1,126 µg/mL which agree
590 with previous studies (0.2–15 mg/L). However, IAA production from both *Streptomyces* and
591 non-*Streptomyces* spp. Actinobacterial isolates with L-tryptophan remain moderate compared
592 to other plant-associated bacterial phyla (Nimnoi et al., 2010). Six isolates comprising RZB13,

AW25, S27, RZB, S28 and AW22 were the highest producers (in the range 16,44±2,05-23,999±1,126 µg/mL). Strain AW22 exhibited maximum IAA production with 23,999±1,126 µg/mL with 0,2% (w/v) L-Trp added. Thus, AW22 was selected for further studies. Moreover, nine isolates, RZBD, AW11, AW01, AW17, RZB11, RZB24, AW08, AW1F2 and AW12 were moderate producers (in the range 8,185±1,045-12,735±1,038 µg/mL) and the rest were the least producers (in the range1,8534± 0,1724- 7,843±0,612µg/mL).

Our findings agree with those described by Abbasi et al. (2019) on the ability of 106 cucumber and tomato rhizosphere-originated actinobacteria to produce ranges of 7.0–40.9 µg/mL of IAA. The same authors declared that twenty percent of test strains had more than 27 µg/mL IAA with 0,5% (w/v) L-Trp. IAA biosynthesis constitutes a common feature amongst rhizospheric *Streptomyces* species. Strains exhibiting antagonistic activity against plant pathogens are concerned by this biosynthesis (Sreevidya et al., 2016). Passari et al. (2016) reported a maximum amount of 43.8 µg ml^{-1} from *S. thermocarboxydus* DBT219, a tomato-associated endophyte (*Solanum lycopersicum*). This production was slightly higher than the minimal concentration reported by Goudjal et al. (2016), ranging from 35.9-117 µg/mL. Nafis et al. (2019) reported IAA amounts evolving from 6.70 to 75.54 µg/mL within eight days of incubation, with a maximum production obtained from *Streptomyces sp.* MNC-1 was originated from the Merzouga desert. Several studies advocated the production of IAA from actinobacteria strains isolated from Algerian niches. Toumatia et al. (2016) described the Saharan soil originated *Streptomyces mutabilis IA1* ability to release a significant amount of IAA at the maximum level of 74.39 (µg ml^{-1}), adding to its biocontrol properties against *Fusarium* and rhizosphere competence. For instance, out of 14 actinomycetes strains isolated from salty water (Sebkha) in Northeast Algeria (Smati and Kitouni, 2019), nine were able to synthesize IAA with variable productivity rates ranging from (7.44 to 21.4 µg/ml). Indeed,

strain *Nocardiopsis aegyptica* H14 recorded the highest score, followed by strains *Nocardiopsis dassonvillei* subsp. *dassonvillei* T45, *Streptomyces xantholiticus* G22 and *Streptomyces iakyrus* G10 with 14.75 µg/ml, 12.37 µg/ml and 12.25 µg/ml, respectively. However, the lowest production amount was recorded by *Streptomyces xantholiticus* G33 at 7.44 µg/ml (Djebaili et al., 2020). These results are slightly lower than those obtained in our study.

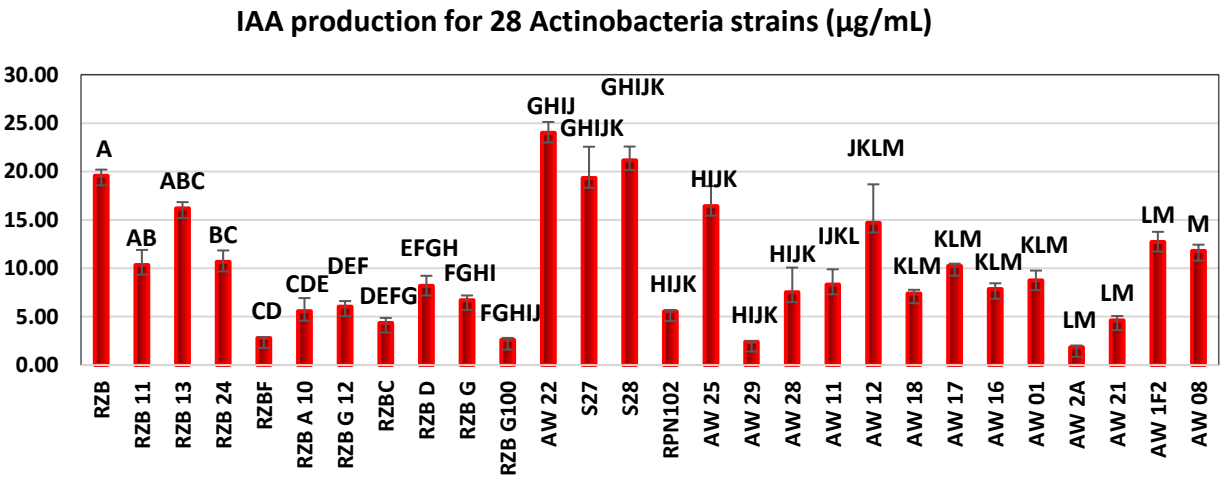

Fig. 2. Screening for IAA production within twenty-eight *Streptomyces*-like strains

Means were contrasted using a one-way ANOVA ($p < 0.05$). Values consist of the average and standard deviations for three biological replicates of each experiment. According to Tukey, values that share a letter within a column are not statistically different.

3.2. Morphological and physiological characterization of AW22

Strain AW 22 displayed typical morphological features of *Streptomyces* genus (van der Aart et al., 2019). The cultural aspects of AW22 are noted in Table 7. Strain AW22 exhibited abundant growth on ISP2, ISP3, ISP5, ISP6 and ISP7, and various pigments were observed on integral test media. Soluble and diffusible pigments from dark brown to navy blue, reddish-orange, and pink to purple were observed on ISP2, ISP3 and ISP5. However, AW 22 growth was moderate on ISP1, good on ISP4 and ISP9, with light blue pigment observed exclusively

on ISP1. Colony diameter and phenotype of aerial mycelium vary from one medium to another, with an abundant coloured sporulation rate observed on all tested media.

Table 7 records the primary physiological and biochemical attributes of AW 22, as these evaluations are critical assets for classifying and identifying actinobacteria. A pH ranging between 5-11 enabled the strain to grow.

No growth at pH13, with optimum growth at pH comprised between 6,8-9.2. Besides, AW22 displayed up to 7% NaCl tolerance. AW 22 was able to grow at temperatures ranging between 15- 40 °C. However, no bacterial development was noticed at 4°C or 45°C. The optimum temperature was revealed to be 28°C. After correlating the physiological and biochemical traits of strain AW 22 to those of model organisms belonging to the genus, the strain was categorized as a *Streptomyces*.

Table 7. Relative cultural characteristics of strain AW 22 on nine *ISP* media.

Medium	**Aerial mycelium**	**Spore color**	**Substrate mycelium**	**Soluble pigment**	**Colony size**	**Growth status**
ISP1	White to light greyish blue	Light blue	Creamy white to light blue	Light blue to green	Small	+
ISP2	Light blue to light grey, then dark grey	Dark grey	Orange to intense brown	Brown, then Navy blue to purple	Big	+++
ISP3	Creamy white to Orange	Dark Grey	Orange, burgundy, then dark brown	Pink to light blue to reddish-purple	Medium	+++
ISP4	Salmon to reddish grey	Light Grey	Orange to red to grey	None	Medium	++

ISP5	Greyish white	Greyish white	Pink to dark red	Pink to purple	Small	+++
ISP6	Creamy to orange	Orange	Creamy white	None	Small	+++
ISP7	Reddish orange to yellow to grey	White to grey	Orange to red to brown	None	Small	+++
ISP9	Creamy white to grey	White to grey	Creamy white	None	Small	++

Note: "+++" indicates growth very good, "++" indicates growth good, "+" indicates growth is moderate, "-" indicates no growth.

3.3. Enzyme production and biochemical characteristics

Phenotyping for enzyme production from the AW 22 strain under *in vitro* conditions showed that most results were positive (Table 8).

Table 8. Enzymatic profile, biochemical and physiological characteristics of strain AW 22.

Enzyme's production	**Result**	**Biochemical tests**	**Result**	**Physiological tests**	**Result**
Amylases	++	Nitrate reductase	++	**Temperature**	
Cellulases	++	Simmons Citrate	+	4°C	-
Lignin oxidases	UD	Peptonisation of Skim milk	+	15°C	+
Xylanases	UD	**Toletrance to [NaCl]**		20°C	++
Urease	+	1%	+++	25°C	+++
Chitinases	+	2%	+++	30°C	+++
Catalase	+	2.5%	+++	35°C	+

Protease (Caseinase)	+	3%	+++	40°C	+/-
Gelatinase	-	4%	+++	45°C	-
Lipase	-	5%	+++	**Tolerance to**	
Lipoproteinases	++	6%	++	Tellurite 0.5%	+
Lecithinase	++	7%	+	Sodium Azide 0.1%	-
Esterase	+	8%	+	Phenol 0.2%	+
Twain 20	+	9%	+	**Growth at**	
Twain 80	+	10%	-	pH5.6	+++
				pH6.8	+++
				pH9.2	+++
				pH11	+++
				pH13	-

Note: In the Enzymes test items, the "+" means positive, "-" indicates negative, and "UD" indicates undetectable activity. In the other tests, "+++" indicates growth very good, "++" indicates growth good, "+" indicates growth is moderate, "-" indicates no growth.

Strain AW 22 showed significant proteolytic activity and produced cellulase, amylase, lipase, lipoproteinase, and esterase activities. Strain AW 22 exhibited nitrate reduction and positive responses to the catalase and urease tests. Amylases, the thermostable enzymes, efficiently degrade organic matter and hasten the composting process (Turan et al., 2017). Through the cleavage of cell wall proteins, microbial proteases play a crucial part in the interactions between the various soil microbiomes (Stach et al., 2018; Vranova et al., 2013). Lipases are extensively prevalent amongst microbes with substantial industrial value since triglycerides' hydrolysis considerably contributes to the composting of sewage sludge (Pascoal et al., 2018).

667 Catalase preserves cells from reactive oxygen species oxidative damages by catalyzing the
668 destruction of hydrogen peroxide into H_2O and O_2. This feature gives the strain remarkable
669 resilience to several external mechanical and chemical limitations (Mushtaq et al., 2019).
670 Furthermore, biosynthesis of the chitinolytic enzymes was detectable in the CCA medium.

671 Actinobacteria strains' enzymatic activities exert a direct phytostimulation and biocontrol of
672 pathogens, thus preventing plant pathologies. Nonetheless, degradation of lignin and Xylan
673 was undetectable in this strain, despite the moderate growth of this strain on their respective
674 test media. Hydrolytic enzymes are essential for improving soil fertility and characteristics.
675 Soil enzymes degrade complex polysaccharides and proteins into simpler molecules (Turan
676 et al., 2017). These enzymes are biotechnologically interesting and of significant commercial
677 value (Islam et al., 2015; Reetha et al., 2014). The chitinolytic activity of *Streptomyces AW 22*
678 may be implicated in the fungal cell wall digestion. The chitinase synthesis effectively
679 inhibits fungal growth. The aptitude of AW22 to secrete chitinases suggests its implication
680 in the biocontrol of fungal phytopathogens and nutrient competition (Gherbawy et al., 2012).
681 However, different mechanisms, like antibiosis, hyperparasitism, and proteolytic and
682 lipolytic enzymes (Xu et al., 2017), are less studied. However, these mechanisms are also
683 involved in the antagonism of plant-associated fungi.

684 **3.4. Plant sugar and nitrogen utilization profile of selected strain**

685 Physiologically, most reported actinomycetes isolates utilised different carbohydrates as the
686 carbon source. This characteristic is pivotal in the actinobacteria taxonomic analysis
687 (Pridham and Gottlieb, 1948). For instance, strain AW 22 efficiently assimilated D-glucose, D-
688 Xylose, D-Galactose, D- Mannose, Maltose, α-Lactose, D-fructose, D- Ribose, L-Rhamnose,
689 Inositol and D-Mannitol. The strain could utilize a low proportion of L-Arabinose, Melibiose,

690 Sucrose and Sorbitol as carbon sources. However, AW 22 was unable to metabolise
691 Raffinose. The results indicate broad carbon assimilation from various vegetal substrates and
692 SCG (Table 9).
693 AW 22 showed an extensive plant sugar utilization profile and a wide array of hydrolytic
694 enzymes. The high proportion of sugars present in SCGs, notably mannose, galactose,
695 glucose, and arabinose, explains the strain's ability to develop on an SCGs extract broth.
696 Further, the IAA production of this strain on SCGs extract has been described for the first
697 time in this report. This multi-functionality of *Streptomyces* strains may be accredited to their
698 large genome and epigenetic factors, such as the location and the high contents of organic
699 matter in wheat fields.
700
701 **Table 9**. Carbon and nitrogen source utilization profile of AW 22.

Carbon test items	**Result**	**Carbon test items**	**Result**	**Nitrogen test items**	**Result**
L-Rhamnose	+++	D-Mannitol	+++	Glycine	+
Sucrose	++	D-Xylose	+++	Tyrosine	+++
D-Glucose	+++	L-Arabinose	+	L-Asparagine	++
Maltose	+++	Raffinose	-	Proline	++
D- Ribose	+++	D- Mannose	++	Casein	++
Melibiose	++	D- Galactose	+++	L-Methionine	+
Lactose anhydrous	+++	Starch	+++		
Inositol	+++	D-Fructose	+++		
Sorbitol	++	α- Lactose	+++		

702 Note: "+++" indicates growth in carbon or nitrogen source is excellent, "++" indicates growth in carbon
703 or nitrogen source is good in general, "+" indicates growth in carbon or nitrogen source is weak, "-"
704 indicates no growth in carbon or nitrogen sources.
705 **3.5. 16S rRNA Gene Sequencing**

706 The AW22-related 16S rDNA sequence was deposited in the NCBI GenBank under the
707 accession ID OP176004. Taxonomical analyses derived from 16S rRNA gene sequencing of
708 AW22, the higher IAA producer, were compared with 98–99,99% similar sequences retrieved
709 from the GenBank database. Sequence alignment confirmed that the strain belongs to the
710 order *Streptomycetales* and the genus *Streptomyces*. 16S rRNA locus similarity calculations,
711 based on neighbour-joining analysis, specified that the neighbouring relatives for strain
712 AW22 were: *S. rubrogriseus* (KX431235) and *S. fradiae* (AB184063) with similarity values of
713 99,22 %, and *Streptomyces violaceoruber* (MH155969) and *Streptomyces lividans* (KY767029) with
714 99.04% similarity. The phylogenetic tree constructed with the neighbour-joining method and
715 Tamura-Nei model is shown in figure 3. Strain AW22 formed an independent clade with *S.*
716 *anthocyanicus* KU973991 separated from *S. rubrogriseus CS3KG4LA166* (OM971238).
717

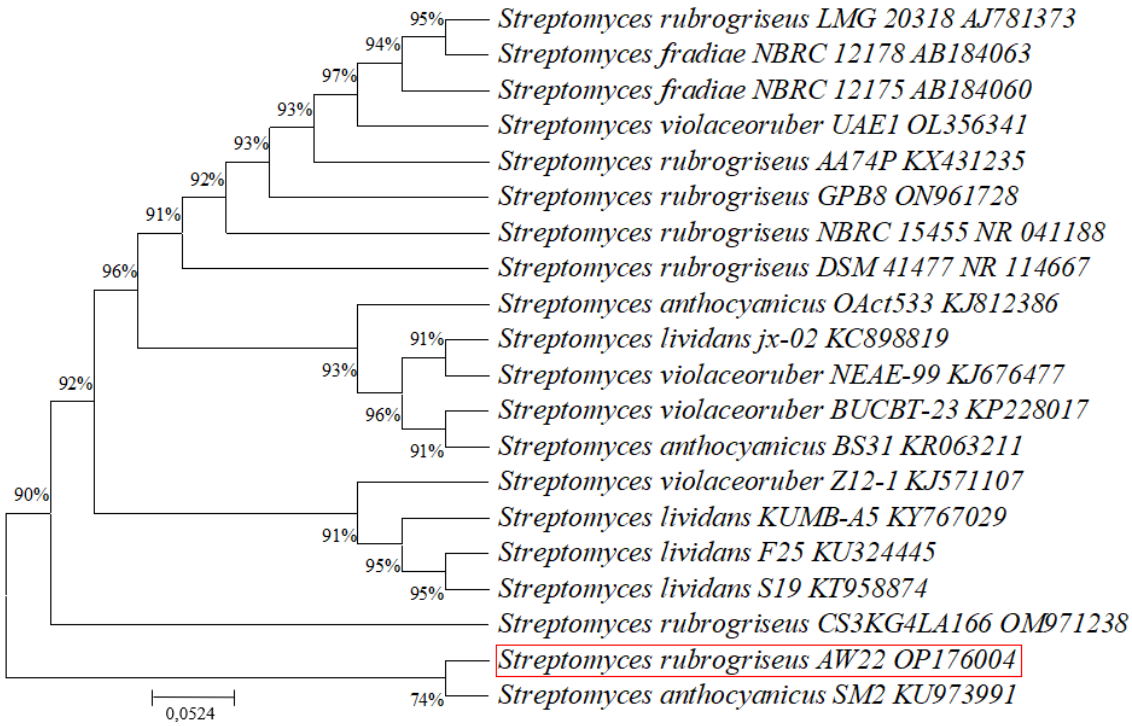

Figure 3. Phylogenetic tree based on NJ method of 16S rRNA gene sequences of *S. rubrogriseus* AW22 and related strains.

Neighbour-joining-based tree displaying the taxonomic position of AW 22 compared to its interrelated *Streptomyces* species. The records at nodes indicate the percentage of replicate trees where associated taxonomic units clustered via the bootstrap test relying on 1000 replicates, with collapsed bootstrap replicates when values < 50%. The *p*-distance served to compute developmental distances representing the units of the number of base differences per site. Less than 50% of placement gaps and alignment openings, incomplete data or ambiguous bases were permitted at any position. Subsequently, positions with < 50% site coverage were eliminated. The scale bar illustrates 0.0524 substitutions per position of nucleotide.

3.6. TLC and HPLC analysis of putative IAA

The spots developed separately on TLC plates were examined under UV light at 245 nm. The findings demonstrated that authentic IAA and presumed IAA fractions isolated with EA from AW 22 filtrate exhibited similar retention factor (RF) values of 0.69.

Likewise, the HPLC profile of the authentic IAA peaked at a retention time of 3.508 min, and putative IAA recovered from AW 22 showed up as a prominent area peak at a comparable retention time of 3.711 min with 0.761 mg/mL, confirming that strain AW 22 produced IAA. These results correspond with preceding studies (Myo et al., 2019).

3.7. Time course of IAA and biomass production from strain AW 22

Changes in biomass and IAA production for AW 22 over ten days of incubation are illustrated in Figure 4. Under optimal conditions, two growth phases of the cycle can be identified from the evolution of biomass, AW 22 cells, a long phase and a short phase.

The strain's growth rate peaked at 712,27±0,4 mg of dry weight on the fifth day of incubation and then stabilized for two days. Thus, the cell dry weight decreased by the seventh day to reach 432,87±1,0 mg. However, the biomass increased again and peaked a second time at 794,47±0,3 mg on the eighth day of incubation, where the germination of new spores may explain this phenomenon. Subsequently, the biomass decreased until the last sampling day.

Furthermore, the IAA synthesis time course of AW 22 was studied over ten days. L-Trp was supplemented with 0.2% (w/v) at an early stage of cell growth. On the first day of incubation, AW22 yielded only 8,84±1,18 µg/mL of IAA followed by a gradual enhancement in IAA secretion parallelly with cell growth over the first seven incubation days to attain 37,52 ±2,18 µg/mL to reach its maximum yield of 41,79± 1,73 µg/mL by the day 9. The growth of *Streptomyces rubrogriseus* AW22 was almost identical whether Trp was present or absent in the medium. Meanwhile, only the cultures fed with Trp exhibited increased IAA content.

The comparison of the evolution of biomass and IAA production indicates that this strain's synthesis of secondary metabolites was closely proportional to cell proliferation.

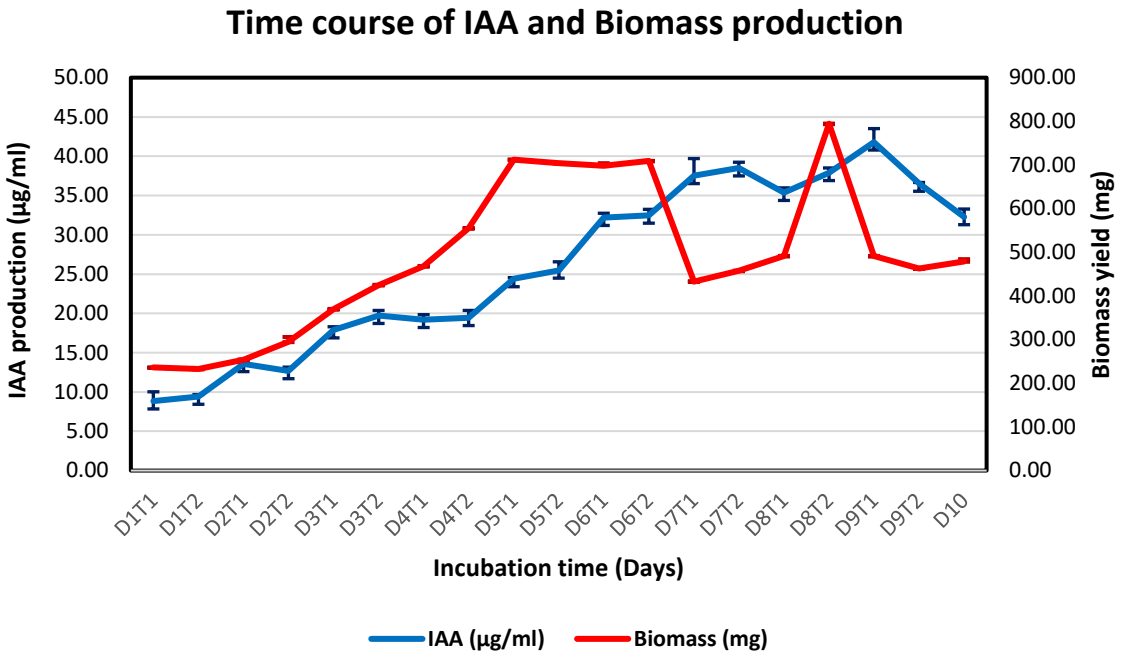

Figure 4. Time course for IAA and Biomass production under standard conditions**.**

3.8. Effect of substrate concentration on IAA production

To attain low-cost IAA production, SCG was preferred as an alternative affordable fermentation substrate to substitute laboratory-grade carbon sources (Tran et al., 2023).

Our previous experiments indicated that GYM broth containing 0.2% L-tryptophan resulted in the maximum IAA yield of 41,79±1,73 µg/mL under optimal media and culture conditions. Subsequently, we briefly assessed the ability of strain AW 22 to produce IAA on a minimal medium containing different carbon sources, ranging from 10-50% for the SCG and CBP and from 0,2-1% for glucose. Depending on the strain, various carbon sources affect IAA production differently. In some cases, different bacteria have other preferences for using

771 sugars, which can also impact auxin production through bacterial growth (Mohite, 2013;
772 Sridevi et al., 2008).

773 Fermentation performed with crude SCG and CBP extracts obtained with the hydrothermal
774 method showed greater IAA yield after the same incubation period (data shown in figure 5).

775

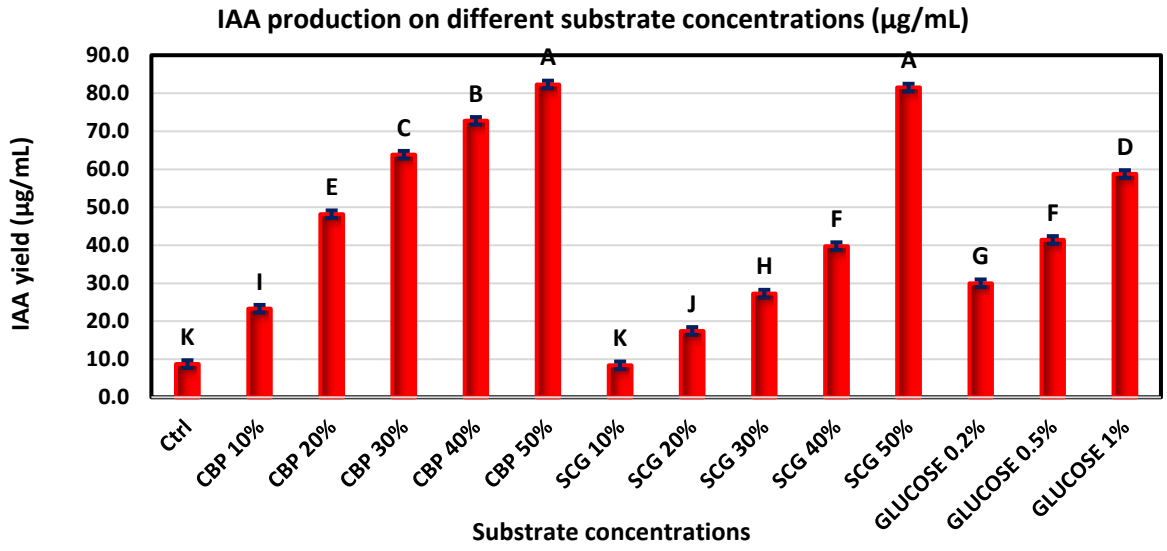

776

777 **Fig.5**. Effect of substrate concentrations on IAA production (µg/mL).
778 Means were contrasted using a one-way ANOVA ($p < 0.05$). Values consist of the average and
779 standard deviations for three biological replicates of each experiment. According to Tukey,
780 values that share a letter within a column are not statistically different.

781

782 The optimal IAA yield was detected at 50% CBP and 50% SCG, with respectively, 82,3 ±2,18
783 µg/mL and 81,5 ±1,47 µg/mL, being 10-fold higher than the negative control and about 2-fold
784 more elevated than the positive control. Nevertheless, no significant difference was
785 observed between both IAA productivity on these two components when they were
786 amended to the medium at a concentration of 50%. Indeed, the greater the concentration of
787 SCG and CBP, the greater the IAA yield from strain AW 22. From the experimental data, we

788 postulate a favourable impact of gradient concentration of CBP and SCG as the only carbon
789 suppliers on IAA synthesis.

790 The glucose concentration had a smaller effect on IAA production than SCG and CBP.
791 Conversely, IAA production was minimal in the medium containing SCG 10% with 8,4±0,14
792 and reaching only 17,5±0,14 µg/ml, 27,3±0,22 µg/mL, 23,3±0,17 µg/ml with SCG 20 %, 30%,
793 CBP 10 %, respectively. Moderate IAA concentrations were obtained in medium containing
794 Glucose 0.2%, SCG 40% and CBP 20% with respectively, 30,0±0,08 µg/mL, 39,8±0,22 µg/mL
795 and 48,2±0,17 µg/mL. Therefore, 30-50% SCG and CBP concentrations were selected for IAA
796 production by strain AW 22.

797 Additionally, the production of IAA was significantly impacted by the precursor Trp, as
798 indicated by the increased IAA level in the positive control consisting of Glucose 0.5%
799 containing L-Trp compared with the negative control devoid of L-Trp. IAA content
800 augmented from 8,7±0,30 to 41,4±0,96 µg/mL in the broth containing 0.2% Trp.
801 These findings suggest that this strain may use both L-Trp dependant and independent
802 pathways to synthesize Auxin in the culture medium. The low amount of IAA produced in
803 the minimal medium from which carbon and nitrogen supplies were omitted demonstrates
804 illustrates how these macronutrients affect the formation of IAA in AW22.
805 The increase in the carbon source (CBP, SCG or glucose) is followed by an increase in IAA
806 productivity. These results advocate the critical role of carbon source concentration and L-
807 Trp serving as a precursor in IAA production. Moreover, it highlights the positive correlation
808 between carbon source concertation and IAA yield. This influence may not be directly
809 related to IAA production but indirectly by stimulating bacterial growth suggested earlier
810 from the kinetic of IAA production and biomass production.

Therefore, carbon sources (CBP and SCG) and L-Trp concentrations were optimized using the following statistical approaches to develop a low-cost medium. A recent study reported similar IAA levels using crude glycerol and feed-grade tryptophan as economic substitutes for analytical-grade glycerol and tryptophan (Bunsangiam et al., 2021). Chaudhary et al. (2021) reported 18.74 mg/L mixing corn flour and soybean meal by *Kosakonia pseudosacchari* TCPS-4. Another report described considerable amounts of IAA (148 µg/ml) produced by *Saccharothrix texasensis* MB15 using wheat wastes (leaves and roots) (Benadjila et al., 2022).

3.9. Influential factors screen using Plackett-Burman design (PBD)

The PBD strategy investigated the fermentation parameters most significantly affecting IAA generation. The previous experiments identified four potentially important variables (SCG, CBP, tryptophan and incubation time) and were subject to the statistical screen with the PBD methodology.

Fig. 6 shows that factor combination 10 exhibited optimum IAA production values, reaching 161,95±3,96 µg/ml. Nonetheless, strain AW22 produced 33,26±2,01 µg/ml from medium composition 4.

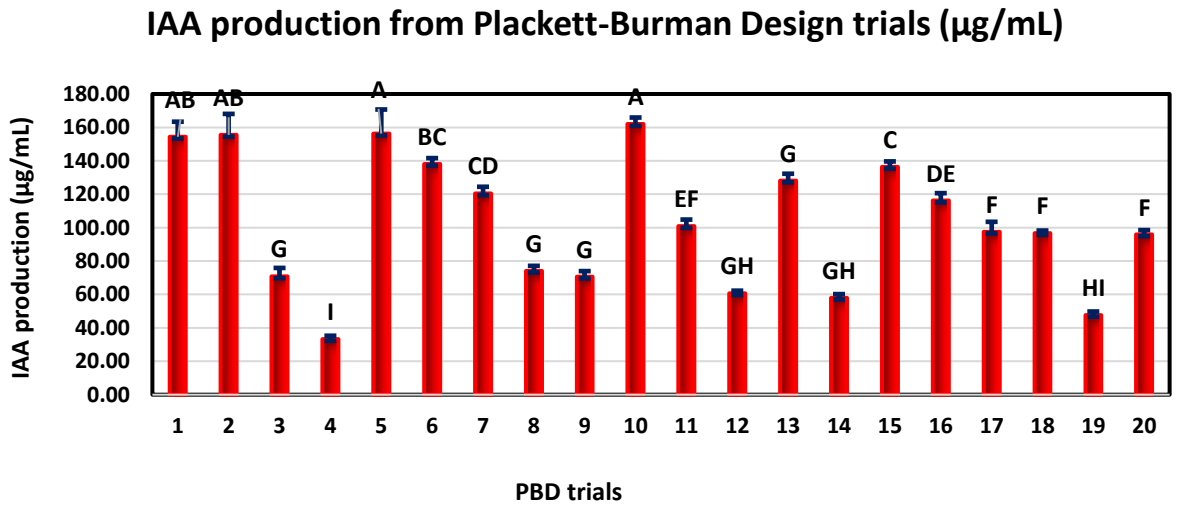

Fig. 6. PBD trials related IAA production (μg/mL).

Means were contrasted using a one-way ANOVA ($p < 0.05$). Values consist of the average and standard deviations for three biological replicates of each experiment. According to Tukey, values that share a letter within a column are not statistically different.

Table 10 records the statistical metrics of the PBD approach and factor effects on Y, the response value (IAA yield). One-way ANOVA clearly indicated that *p*-values for SCG, tryptophan, pH and temperature were significant (0,031, 0,001, 0,010 and 0,006, respectively). This analysis indicates that among the fourteen variables, these four factors are key parameters impacting the IAA yield and were identified as critical factors for the RSM approach.

Temperature is a physiological factor affecting fermentation and ATP regulation (Yan et al., 2018). High or low temperatures may impact the biological activity of actinomycetes due to their slow growth (Kanimozhi et al., 2017; Sohn et al., 2023). In turn, this variation modulates the regulatory metabolic pathways and the constitution of the cell wall, resulting in a variety of metabolic responses and the synthesis of a wide array of products (Talukdar et al., 2016).

Different IAA biogenesis pathways are evolutionary in microbiomes and their host plants. Di et al. (Di et al., 2016) outlined distinct IAA biosynthesis pathways in multiple species. Contrary to nutritional effects, Trp has a crucial role in almost all bacterial strains that produce IAA. Tryptophan monooxygenase converts Trp to indole-3-acetamide before being processed into IAA via indole acetamide hydrolase. The iaaM gene codes for tryptophan monooxygenase, whereas the iaaH gene codes for indole acetamide hydrolase (Casanova et al., 2005; Park et al., 2021). Scientists reported three additional Trp-dependent pathways. According to reports, plants can maintain a baseline level of Auxin through Trp-independent pathways (Ribnicky et al., 2002).

Trp is typically required for bacteria to produce IAA, but the ideal concentration and maximum productivity depend on the species. Nevertheless, investigations on these bacterial IAA biosynthesis pathways are scarce. Additionally, researchers have not fully characterised the Trp-independent pathway in plants (Di et al., 2016).

Nonetheless, the *p*-values for CBP, Starch, Tryptone, Yeast E, NaCl, K_2HPO_4, $MgSO_4$, $CaCO_3$, Incubation time and Inoculation amount % were > 0,05, and none of these variables was significant. Therefore, in the subsequent RSM analysis, these elements weren't excluded from the culture medium but kept at their central (zero) level in the following RSM experiment.

The factors with the most significant influence on IAA productivity are summarized in the Pareto chart (Figure 7) (Hymavathi et al., 2010).

The *t*-value indicates each factor's positive and negative effects (Talhi et al., 2022). A positive value indicates that the factor positively impacts IAA yield; if the value is negative, the opposite is true. Table 10 demonstrates that SCG, Tryptone, L-Trp, NaCl, $MgS0_4$, Inc. Time, T°, pH, and Inoculation amount had positive effects on the IAA production, while the CBP, Starch, Yeast E, K_2HPO_4, $CaCO_3$ had adverse effects.

Organic and inorganic sources of nitrogen also impact IAA productivity by bacteria differently. According to Chandra et al. (2018), combining dextrose and beef extract as carbon and nitrogen sources was optimal for higher IAA productivity. Nonetheless, organic and inorganic nitrogen sources had no significant effect on IAA production from strain AW 22.

The variance of the actual response was explained accordingly with the decision coefficient R^2 values to verify the accuracy and fitness of the model. The model's ability to explain the variation in dependent variables reduces as the R-squared value decreases. In our case, R^2 values could account for 95% of the variation in the data (the model could not explain only

878 5% of the variation), indicating the suitability of the analysis and prediction of changes in
879 IAA generation during fermentation.

880

881 **Table 10**. ANOVA analysis and coded coefficients of the tested factors for IAA production.

Terms	**Fd**	**SS**	**SM**	**Effect**	**Coef**	**SE Coef**	**T-value**	**F-value**	***p*-Value**
Model	14	28449,8	2032,1					6,78	0,022
Linear	14	28449,8	2032,1					6,78	0,022
Constant					103,67	3,87	26,78	0,00	0,000
X1: CBP (%)	1	0,4	0,4	-0,29	-0,14	3,87	-0,04	8,85	0,972
X2: SCG (%)	1	2651,2	2651,2	23,03	11,51	3,87	2,97	0,04	0,031
X3: Starch	1	13,1	13,1	-1,62	-0,81	3,87	-0,21	1,70	0,843
X4: Tryptone (g/L)	1	509,6	509,6	10,10	5,05	3,87	1,30	0,01	0,249
X5: Yeast E (g/L)	1	3,3	3,3	-0,81	-0,41	3,87	-0,11	41,16	0,920
X6: L-Trp (%)	1	12332,9	12332,9	49,66	24,83	3,87	6,42	0,22	0,001
X7 : NaCl (g/L)	1	67,3	67,3	3,67	1,83	3,87	0,47	0,55	0,656
X8: K2HPO4 (g/L)	1	164,0	164,0	-5,73	-2,86	3,87	-0,74	0,30	0,493
X9: MgSO4 (g/L)	1	90,4	90,4	4,25	2,13	3,87	0,55	1,94	0,606
X10 : CaCO3 (g/L)	1	580,6	580,6	-10,78	-5,39	3,87	-1,39	3,57	0,223
X11: Incub. Time (Days)	1	1068,3	1068,3	14,62	7,31	3,87	1,89	20,32	0,118
X12: T°	1	6088,2	6088,2	34,89	17,45	3,87	4,51	16,20	0,006
X13: pH	1	4854,4	4854,4	31,16	15,58	3,87	4,03	0,09	0,010
X14: Inoc. amount %	1	26,0	26,0	2,28	1,14	3,87	0,29	6,78	0,780
Error	5	1498,2	299,6						
Total	19	29948,0							
Model	**S**	**R^2**	**R^2 (prév)**						
	17,3102	95,00%	19,96%						

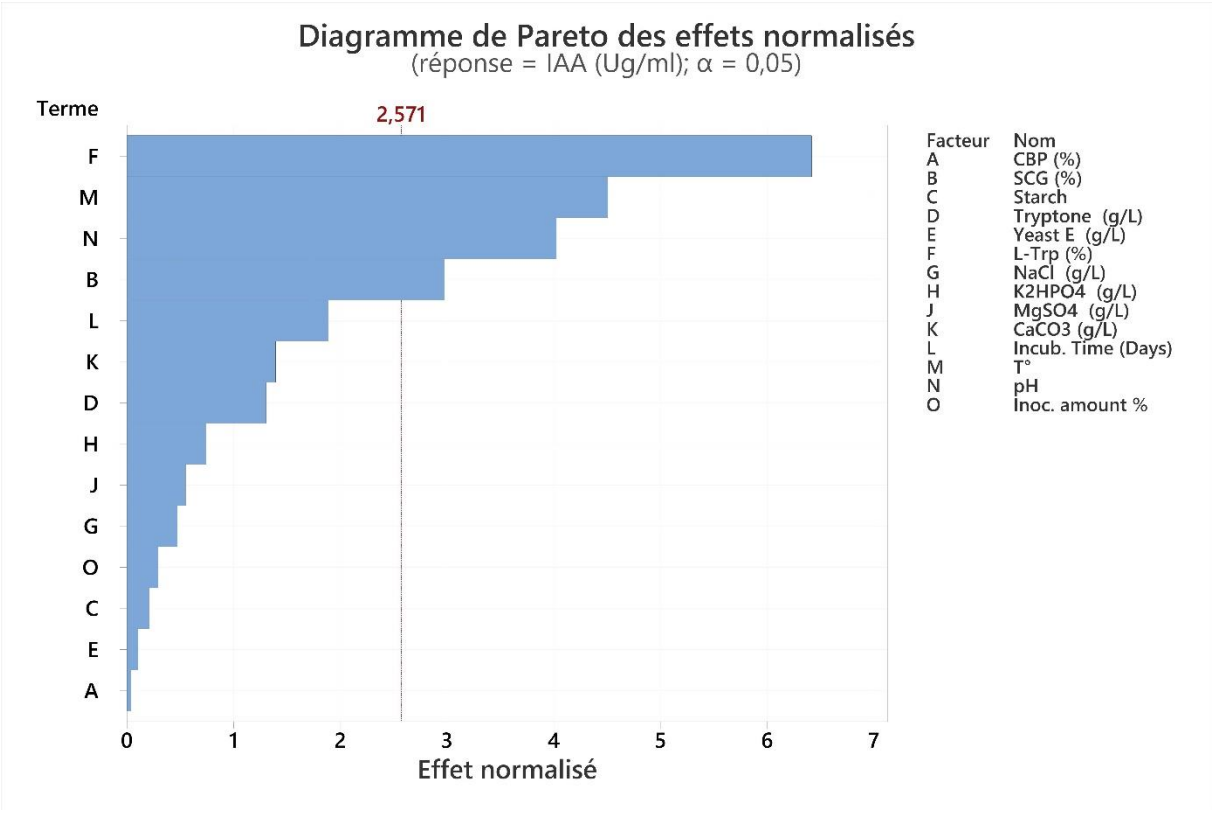

Fig. 7. Pareto chart describing the normalized effects for IAA production.

3.10. Modeling using the RSM-BBD

The microbial fermentation process is complex, nonlinear, and unstructured. The yields of specific compounds can be affected by slight changes in the fermentation media composition and the operating culture parameters, altering the strain's metabolic profile (Kaur et al., 2014). Ideal fermentation conditions can be challenging to determine, requiring experimental designs. RSM helps improve the culture medium composition and operating conditions, enhance IAA productivity and participate in the search for natural physiologically active substitutes for chemical agro-actives (Arul Jose and Jebakumar, 2014; Mazarei et al., 2017).

The primary function of the Box-Behnken experimental design from RSM is to forecast which suitable quadratic model will better elucidate the correlation between inputs and outputs. BBD was carried out to optimise further the concentration of the four factors defined as significant using PBD analysis at three levels to identify the best fermentation conditions for the low-cost process. Figure 8 shows the IAA yield obtained from BBD trials.

In this design, run 12 comprising in (w/v) L-Trp, 0,6% and SCG, 30% with T°, 30,5 and pH 8,05 was ideal for IAA secretion, peaking to 184,36±7,85 µg/mL. Nonetheless, the least IAA amount of 18,56±1,26 µg/mL was notied in run 11 containing (w/v) L-Trp, 0,2% and SCG, 40% with T°, 35 and pH 8,05, which is about 10-fold.

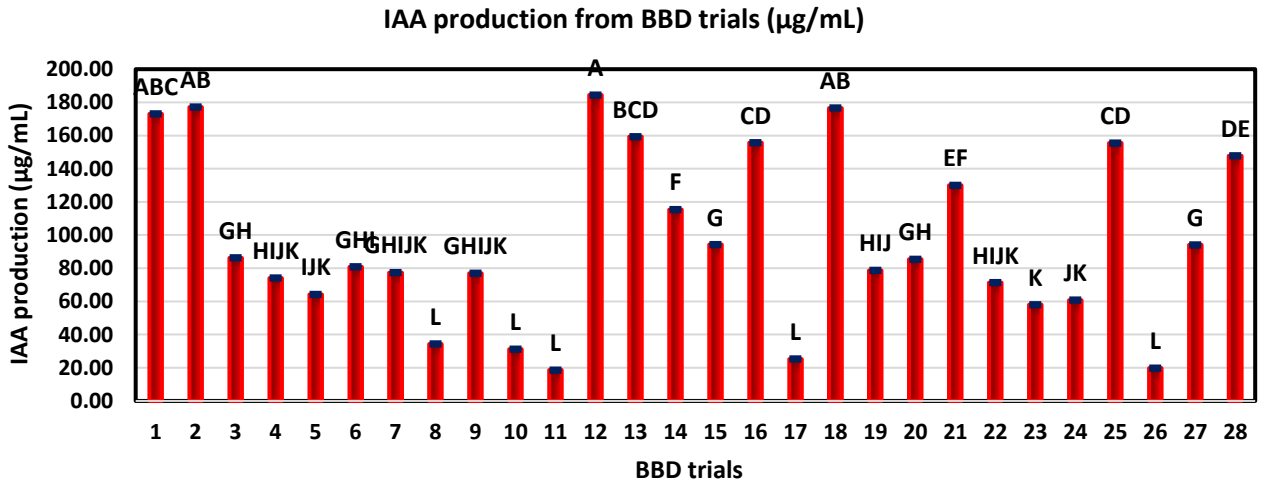

Fig. 8. IAA production according to BBD trials (µg/mL).

Means were contrasted using a one-way ANOVA ($p < 0.05$). Values consist of the average and standard deviations for three biological replicates of each experiment. According to Tukey, values that share a letter within a column are not statistically different.

3.11. Postulated model and statistical validation

The statistical metrics of factor significance, the coded coefficients of variables and other model details obtained from ANOVA are summarized in table 11. In contrast, table 4 lists the actual and predicted response values for IAA productivity.

Table 11. Statistical metrics of the tested factors on IAA production for BBD experiment.

Terms	Fd	SS	SM	Coef	SE Coef	T-value	F-value	*p*-Value
Modèle	14	55808,6	3986,3				2,99	0,028
Linear	4	42806,9	10701,7				8,02	0,002
Constant				120,3	18,3	6,58	0,000	0,000
L-Trp	1	30105,5	30105,5	50,1	10,5	4,75	0,000	0,000
T°	1	2309,5	2309,5	-13,9	10,5	-1,32	0,211	0,211
pH	1	7042,6	7042,6	24,2	10,5	2,30	0,039	0,039
SCG	1	3349,3	3349,3	-16,7	10,5	-1,58	0,137	0,137
Squares	4	6422,4	1605,6				1,20	0,356
L-Trp*L-Trp	1	4081,5	4081,5	-26,1	14,9	-1,75	3,06	0,104
T°*T°	1	3188,5	3188,5	-23,1	14,9	-1,55	2,39	0,146
pH*pH	1	149,8	149,8	-5,0	14,9	-0,33	0,11	0,743
SCG*SCG	1	6,6	6,6	-1,0	14,9	-0,07	0,00	0,945
Interactions	6	6579,3	1096,6				0,82	0,573
L-Trp*T°	1	901,7	901,7	-15,0	18,3	-0,82	0,68	0,426
L-Trp*pH	1	1084,1	1084,1	16,5	18,3	0,90	0,81	0,384
L-Trp*SCG	1	2314,4	2314,4	-24,1	18,3	-1,32	1,73	0,211
T°*pH	1	0,4	0,4	-0,3	18,3	-0,02	0,00	0,987
T°*SCG	1	1117,5	1117,5	16,7	18,3	0,91	0,84	0,377
pH*SCG	1	1161,2	1161,2	17,0	18,3	0,93	0,87	0,368
Error	13	17357,1	1335,2					

Lack of fit	10	8597,1	859,7		0,29	0,938
Pure error	3	8760,1	2920,0			
Total	27	73165,8				

Model	**S**	**R^2**	**R^2 (adj)**	**R^2 (pred)**
	36,5399	76,28%	50,73%	11,03%

A *p*-value of less than 0,05 reveals the significance of the model. Furthermore, the probability value also shows that the model suits and fits the experimental data. Nevertheless, the low model F-value of 2,99 suggests a low model accuracy.

3.12. Factors effects and fitted model

From these data, the model terms L-Trp and pH were significant (p<0,05), while values greater than 0,1000 were insignificant. The linear effects were substantial, as revealed by the monomial coefficients L-Trp and pH having a *p*-value less than 0,05. The other terms' *p*-value was greater than 0,05, indicating a negligible linear impact. The lack of a significant interaction between L-Trp and pH shows no interaction between the two variables.

Moreover, an F-value and a *p*-value of the lack of fit of the response function are respectively 0,29 and 0,938, suggesting the model fitting was not satisfying. In our investigation, the F_0 of 0,29 is inferior to *Fcritic* (0.05, 10.3) = 8.79. Therefore, we cannot settle that the model does not adequately fit the data in this instance (Montgomery, 2019).

An ANN-GA modeling based on nonlinear regression will be implemented to understand the given data further. The determination coefficient R-squared, which had a value of 76,28% and indicated that the model did not account for 23,72% of the total variation in IAA

production, was used to evaluate the significance and correctness of the model developed in this study. The adj R^2 value of 50,73% indicates low reliability between the experimental output values and those predicted by the model. These results further demonstrated the model's low accuracy, suggesting that the equation used to create the model does not suitably reflect the test value. As a result, the regression model was assumed to not adequately and effectively analyze and predict the IAA generation of the *S. rubrogriseus* AW 22.

The regression was conducted to fit the response function to the empirical data. Subsequently, the second-order polynomial regression equation analyzing the regression model and describing the predicted response (Y_{pred}=IAA in μg/mL) generated from RSM is represented as follows (Eq. 14).

IAA (μg/mL) = 120,3 + 50,1 L-Trp - 13,9 T° + 24,2 pH - 16,7 SCG - 26,1 L-Trp*L Trp- 23,1 T°*T° - 5,0 pH*pH - 1,0 SCG*SCG - 15,0 L-Trp*T° + 16,5 L-Trp*pH - 24,1 L-Trp*SCG - 0,3 T°*pH + 16,7 T°*SCG + 17,0 pH*SCG (Eq. 14)

3.13. Contour plots

The contour plots (2D) in Figure 9 designate the graphical representation of the correlations between the significant process factors, optimal values and the specific output variability (Baş and Boya, 2007). These graphics help understand and describe the two variables' combined effect on IAA production by AW 22. According to the contour plot forms, it is possible to instantly verify the significance of the interaction, which may be high if the contour plot is elliptical and saddle or, on the contrary, low if it represents a circular shape

(Berkani et al., 2019). At the same time, the remaining pair of factors were kept at their centre point, thus efficiently determining the maximum response value under the influence of the operating inputs.

The contour plots are elliptical, describing the significant impact of interactions between T°-L-Trp, pH- L-Trp and SCG- L-Trp. The maximum IAA yield was achieved at low temperatures, and high L-Trp with pH and SCG were fixed at the zero level, as shown in figure 9 (a). However, figure 9 (b) explains a maximum production at alkaline pH and high L-Trp concentration. Moreover, when SCG concentration was low and accompanied by a high concentration of the precursor L-Trp, IAA reached its maximum level, as shown in figure 9 (c). Elliptical interactions were also noticed for (pH, T°), (SCG, T°), represented respectively in figure 9 (d), (e), inform that low T° with alkaline pH and low T° with low SCG concentration respectively can lead to elevated IAA concentrations. For SCG and pH, represented in figure 9 (f), contour lines were rounded, suggesting the absence of significance.

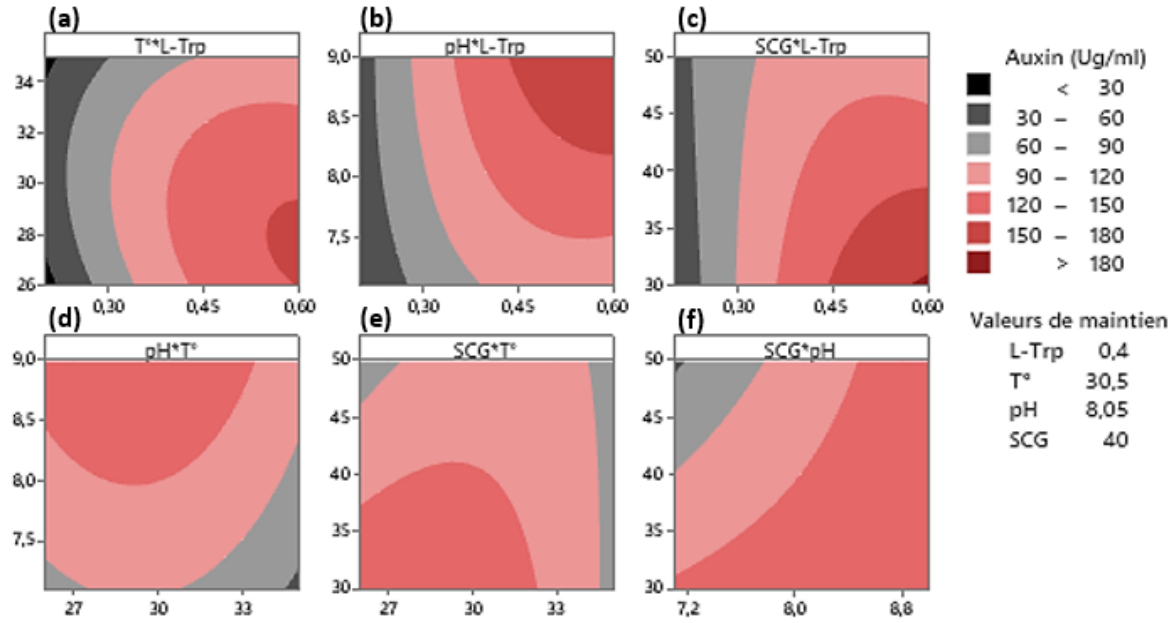

974

975 **Fig. 9**. Contour plots of the IAA production implicating binary independent variables as the

976 coordinates.

977 **3.14. Process modeling using ANN-GA**

978 The primary motive of this study resides in developing a suitable ANN model for the IAA
979 production process using SCG as a low-cost culture medium while minimizing the average
980 error calculated between actual and predicted output values (Smaali et al., 2021)

981 The BBD experimental data (Table 4) and an extra forecasted data set points (200) generated
982 from the second-order polynomial regression equation (Eq. (13)) were processed to create an
983 accurate, robust and reliable ANN model. These data sets were carefully divided into three
984 segments: training (70%), testing (15%), and validating (15%).

985 To prevent over-fitting data, the ANN was trained using a maximal set of data, along with
986 self-tests and validations at each iteration. The ANN's global performance will vary
987 depending on the transfer functions implemented to train the network (Bhattacharya et al.,

988 2017). Thus, in this investigation, both the tangent-sigmoidal transfer function and the pure-
989 linear transfer function at the hidden layer node and at the output layer node, respectively,
990 were applied. Thus, these functions were more efficient than others by giving the lowest
991 MSE and the highest R^2 values.

992 The suitable number of hidden neurons was carefully chosen according to previous studies
993 since the number of hidden neurons significantly affects simulation performance and the
994 ideal network topology (Dhanarajan et al., 2014). The process of modeling is slow when
995 number of neurons is low. Contrarily, extra neurons result in over-fitting, reflected by
996 absorbing the noise in the data needed for training the network, which reduces the
997 robustness and generalizability of the ANN model (Fan et al., 2017).

998 Therefore, the "*trial-error minimization*" approach was employed to select the optimal hidden
999 neurons' number (Ebtehaj and Bonakdari, 2013). This approach compares the calculated
1000 network error with the output. It continuously adjusts the training network's weights and
1001 biases until it reaches the lowest MSE achievable for a specific number of hidden neurons.
1002 For modeling the IAA production process, (1–10) hidden neurons were tested to select the
1003 optimal network topology according to the MSE value/number of neurons relationship.

1004 The one hidden layer standard multilayer feed-forward network has been considered a
1005 universal approximator (Lin et al., 2021; Zhang and Pan, 2014). However, this study
1006 configures the model with two hidden layers.

1007 According to figure 10 (a,b), the training converged after 129 epochs with the lowest mean
1008 square error. Thus, upon iterative training of the ANN, the model achieved a maximum R-
1009 value of 0,999 (Figure 10a) along with a minimum MSE value of $1{,}86\times10^{-5}$ (Figure 10b) at 129

epochs for 6 neurons in the hidden layer with tangent-sigmoidal transfer function. Therefore, the best network architecture of 4-6-1 is used for process optimization, representing 4 inputs in the first layer, 6 neurons in the hidden layer, and one output in the last layer. The R^2 value close to 1 and a low MSE value indicate that the performance of the developed model was satisfying and suitably fits the IAA experimental values.

(a)

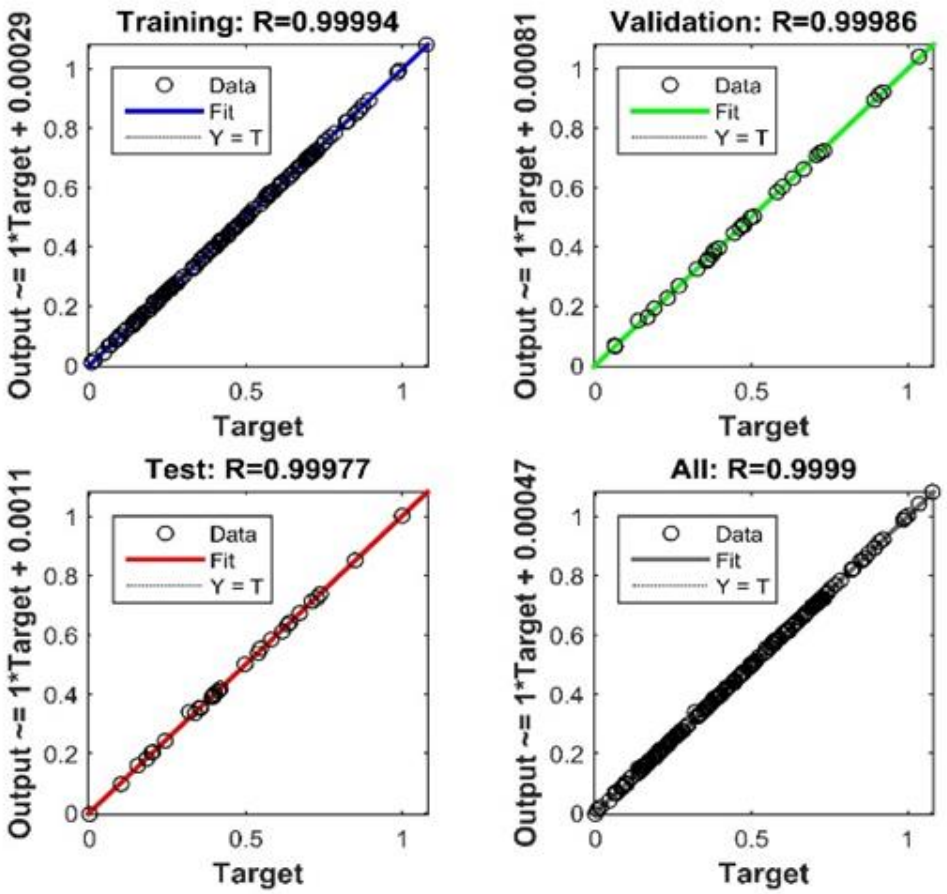

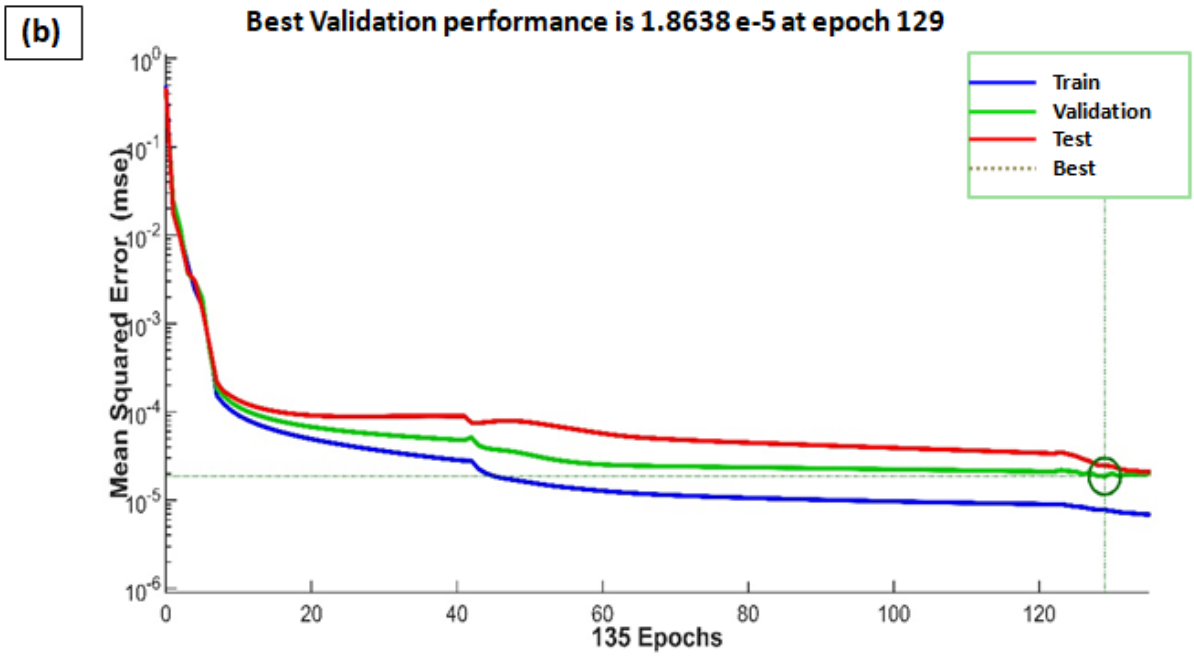

Fig. 10. (a) Regression plot illustrating the correlation between predicted and experimental output values; (b) Performance of the ANN model at the training's last stage exhibiting an MSE of $1{,}86\times10^{-5}$ at 129 epochs.

3.15. GA-assisted optimization

Additionally, the GA algorithm was operated to optimize the ANN model and locate the operating conditions' stationary points that would provide the maximum IAA yield. The GA approach used temperature, initial pH, initial concentration of L-Trp, and SCG as the input parameters to optimize, starting with a population of random regimes. The optimum points of the process variables were selected between the lower and upper ranges presented earlier in table 3. The findings revealed that the maximal IAA level was 226,04 μg/mL under the optimized conditions of the four variables, summarized in table 12.

3.16. Experimental validation of results

The reliability of both postulated models to predict maximum output data was confirmed. For occurrence, triplicate experiment sets were conducted considering the conclusions of RSM-assisted optimization using the desirability function and the ANN-GA-predicted optimal levels of process parameters. Experimental output values were subsequently contrasted with their corresponding simulated responses predicted by the RSM-BBD and ANN-GA modeling.

Predicted optimum levels of inputs, adjusted target output values, and actual response values for RSM-BBD and ANN-GA postulated models are illustrated in table 12.

Table 12. Factors configuration with the predicted and experimental response values.

Factors	**Actual value of predicted optimum**	**Predicted max. Y value (µg/mL)**	**Desirability**	**Expreimental Y value (µg/mL)**
		RSM-BBD		
L-Trp	0,572	184,363	1	183,45±0,18
T°	31,25			
pH	9			
SCG	30			
		ANN-GA		
L-Trp	0,6	226,04		188,290±0,38
T°	25,8			
pH	9			
SCG	30			

1042 According to table 12, the experimentally recorded IAA was 183,45±0,18 μg/mL, which was
1043 close to the predicted value (184,363 μg/mL) for the RSM-BBD model. For the ANN-GA, the
1044 observed IAA concentration obtained from validation experiments (188,290±0,38) closely
1045 matched the expected value (226,04 μg/mL) with a slight difference, suggesting the adequacy
1046 and validity of the model. However, the optimums obtained from ANN-GA permitted an
1047 even higher IAA yield than with RSM-BBD-based modeling.

1048 Moreover, strain AW22 produced substantially more IAA while utilizing the improved
1049 medium. Enhancement in IAA productivity was up to 4,55-fold and 4,46-fold with ANN-GA
1050 and RSM, respectively, compared with the one obtained using the unoptimized
1051 medium. This difference between predicted and experimental values may not only be due to
1052 the genotyping source but also some epigenetic factors such as medium characteristics. We
1053 speculate that this value is the maximum value that strain AW22 can achieve on an SCGs
1054 medium.

1055 The ANN-GA presents higher prediction accuracy in terms of IAA response prediction, the
1056 higher R^2 and the lower MSE compared to RSM, regarding the neglected possibility of the
1057 model getting into overfitting or underfitting after optimization. This performance is
1058 attributed to the overall ability of ANN-GA to analyze the nonlinear behaviour of the
1059 system. At the same time, the response surface model is limited by second-order polynomial
1060 regression. Therefore, these findings confirm the suitability of the ANN-GA assisted
1061 modelisation as an alternative to RSM-based models in predicting microbial metabolic
1062 profiles, such as IAA.

1063

4. Conclusion

Reports on the effective IAA production from rhizospheric and endophytic *Streptomyces* strains are growing. Nonetheless, this is the first report on *Streptomyces rubrogriseus* AW 22 isolated for the first time from wheat rhizosphere in the unexplored region of Tiffeche in the Souk-ahras province in Algeria. Moreover, this is the first study exploring its IAA production potential that has never been reported till now. AW 22 showed pertinent enzymatic activities and unique pigments on various culture media. Moreover, this study describes the valorization of SCGs for *in vitro* and *in silico* low-cost medium engineering with machine learning tools such as RSM and ANN-GA. This novel advanced approach aims to maximize organic IAA production using SCG hydrothermal extract as a low-cost substrate to predict optimal operation conditions for maximizing IAA yield while minimizing the process costs and reducing the processing time and the number of experiments. These findings demonstrate the higher reliability ANN-GA-based model compared to RSM. The reason may be due to microbial growth and metabolism's nonlinear and complex characteristics. The multi-functionality of *S. rubrogriseus* AW 22 opens up new prospects in agricultural management approaches as organic plant growth promoters and its production at the industrial scale. Thus, it is essential to elaborate a metabolic profile for AW 22, to investigate its plant nutrient uptake improvement, such as phosphate solubilization, and to evaluate the strain's *in vivo* biocontrol potential of soil-borne pathogens.

This investigation gives exciting insights into the possible orientation of this bioprocess into large-scale industrial production of Streptomyces-originated IAA for commercial purposes, with an ambition to formulate a product with an extended shelf life. Furthermore, formulation assays of the strain's biomass will be an asset. Thus, determining the IAA biosynthetic pathway in this strain would be the object of future investigation.

References

Abbasi, S., Safaie, N., Sadeghi, A., Shamsbakhsh, M., 2019. Streptomyces Strains Induce Resistance to Fusarium oxysporum f. Sp. Lycopersici Race 3 in Tomato through Different Molecular Mechanisms. Front. Microbiol. 10, 1505. https://doi.org/10.3389/fmicb.2019.01505

Abdelmoteleb, A., Troncoso-Rojas, R., Gonzalez-Soto, T., González-Mendoza, D., 2017. Antifungical activity of autochthonous Bacillus subtilis isolated from prosopis juliflora against phytopathogenic fungi. Mycobiology 45, 385–391. https://doi.org/10.5941/MYCO.2017.45.4.385

Agarwal, S., Tyagi, I., Gupta, V.K., Ghaedi, M., Masoomzade, M., Ghaedi, A.M., Mirtamizdoust, B., 2016. Kinetics and thermodynamics of methyl orange adsorption from aqueous solutions—artificial neural network-particle swarm optimization modeling. J. Mol. Liq. C, 354–362. https://doi.org/10.1016/J.MOLLIQ.2016.02.048

Aghaeinejad-Meybodi, A., Ebadi, A., Shafiei, S., Khataee, A., Kiadehi, A.D., 2019. Degradation of Fluoxetine using catalytic ozonation in aqueous media in the presence of nano-Γ-alumina catalyst: Experimental, modeling and optimization study. Sep. Purif. Technol. 211, 551–563. https://doi.org/10.1016/j.seppur.2018.10.020

Ahirwar, S., Soni, H., Prajapati, B.P., Kango, N., 2017. Isolation and screening of thermophilic and thermotolerant fungi for production of hemicellulases from heated environments. Mycology 8, 125–134. https://doi.org/10.1080/21501203.2017.1337657

Al Farraj, D.A., Varghese, R., Vágvölgyi, C., Soliman Elshikh, M., Alokda, A.M., Hossam Mahmoud, A., 2020. Antibiotics production in optimized culture condition using low cost substrates from Streptomyces sp. AS4 isolated from mangrove soil sediment. J. King Saud Univ. - Sci. 32, 1528–1535. https://doi.org/10.1016/j.jksus.2019.12.008

Aleboyeh, A., Kasiri, M.B., Olya, M.E., Aleboyeh, H., 2008. Prediction of azo dye decolorization by UV/H2O2 using artificial neural networks. Dye. Pigment. 77, 288–294. https://doi.org/10.1016/J.DYEPIG.2007.05.014

Arul Jose, P., Jebakumar, S.R.D., 2014. Successive Nonstatistical and Statistical Approaches for the Improved Antibiotic Activity of Rare Actinomycete Nonomuraea sp. JAJ18. Biomed Res. Int. 2014. https://doi.org/10.1155/2014/906097

Bagheri, M., Mirbagheri, S.A., Bagheri, Z., Kamarkhani, A.M., 2015. Modeling and optimization of activated sludge bulking for a real wastewater treatment plant using hybrid artificial neural networks-genetic algorithm approach. Process Saf. Environ. Prot. 95, 12–25. https://doi.org/10.1016/j.psep.2015.02.008

Bano, N., Musarrat, J., 2003. Characterization of a new Pseudomonas aeruginosa strain NJ-15 as a potential biocontrol agent. Curr. Microbiol. 46, 324–328. https://doi.org/10.1007/s00284-002-3857-8

Baş, D., Boya, I., 2007. Modeling and optimization I: usability of response surface methodology. J Food Eng 78, 836–845. https://doi.org/10.1016/j.jfoodeng.2005.11.024

Benadjila, A., Zamoum, M., Aouar, L., Zitouni, A., Goudjal, Y., 2022. Optimization of cultural conditions using response surface methodology and modeling of indole-3-acetic acid production by Saccharothrix texasensis MB15. Biocatal. Agric. Biotechnol. 39, 102271. https://doi.org/10.1016/j.bcab.2021.102271

Berkani, M., Bouhelassa, M., Bouchareb, M.K., 2019. Implementation of a venturi photocatalytic reactor: Optimization of photodecolorization of an industrial azo dye. Arab. J. Chem. 12, 3054–3063. https://doi.org/10.1016/j.arabjc.2015.07.004

Bhattacharya, S., Dineshkumar, R., Dhanarajan, G., Sen, R., Mishra, S., 2017. Improvement of ε-polylysine production by marine bacterium Bacillus licheniformis using artificial neural network modeling and particle swarm optimization technique. Biochem. Eng. J. 126, 8–15. https://doi.org/10.1016/j.bej.2017.06.020

Boubekri, K., Soumare, A., Mardad, I., Lyamlouli, K., Hafidi, M., Ouhdouch, Y., Kouisni, L., 2021. The screening of potassium-and phosphate-solubilizing actinobacteria and the assessment of their ability to promote wheat growth parameters. Microorganisms 9, 1–16. https://doi.org/10.3390/microorganisms9030470

Bulak, P., Walkiewicz, A., Brzezińska, M., 2014. Plant growth regulators-assisted phytoextraction. Biol. Plant. 58, 1–8.

Bunsangiam, S., Thongpae, N., Limtong, S., Srisuk, N., 2021. Large scale production of indole-3-acetic acid and evaluation of the inhibitory effect of indole-3-acetic acid on weed growth. Sci. Rep. 11, 1–13. https://doi.org/10.1038/s41598-021-92305-w

Buono, M.A., Erickson, L.E., 1985. Rapid Measurement of Candida utilis Dry Weight with Microwave Drying. J. Food Prot. 48, 958–960. https://doi.org/10.4315/0362-028x-48.11.958

Casanova, E., Trillas, M.I., Moysset, L., Vainstein, A., 2005. Influence of rol genes in floriculture. Biotechnol. Adv. 23, 3–39. https://doi.org/10.1016/J.BIOTECHADV.2004.06.002

Çelekli, A., Bozkurt, H., Geyik, F., 2013. Use of artificial neural networks and genetic algorithms for prediction of sorption of an azo-metal complex dye onto lentil straw. Bioresour. Technol. 129, 396–401. https://doi.org/10.1016/j.biortech.2012.11.085

Chandra, S., Askari, K., Kumari, M., 2018. Optimization of indole acetic acid production by isolated bacteria from Stevia rebaudiana rhizosphere and its effects on plant growth. J. Genet. Eng. Biotechnol. 16, 581–586. https://doi.org/10.1016/J.JGEB.2018.09.001

Chaudhary, T., Yadav, D., Chhabra, D., Gera, R., Shukla, P., 2021. Low - cost media engineering for phosphate and IAA production by Kosakonia pseudosacchari TCPS - 4 using Multi - objective Genetic Algorithm (MOGA) statistical tool. 3 Biotech 11, 1–11. https://doi.org/10.1007/s13205-021-02690-2

Desai, K.M., Survase, S.A., Saudagar, P.S., Lele, S.S., Singhal, R.S., 2008. Comparison of artificial neural network (ANN) and response surface methodology (RSM) in fermentation media optimization: Case study of fermentative production of scleroglucan. Biochem. Eng. J. 3, 266–273. https://doi.org/10.1016/J.BEJ.2008.05.009

Desai, K.M., Vaidya, B.K., Singhal, R.S., Bhagwat, S.S., 2005. Use of an artificial neural network in modeling yeast biomass and yield of β-glucan. Process Biochem. 40, 1617–1626. https://doi.org/10.1016/J.PROCBIO.2004.06.015

Dhanarajan, G., Mandal, M., Sen, R., 2014. Regular Article. Biochem. Eng. J. C, 59–65. https://doi.org/10.1016/J.BEJ.2014.01.002

Di, D.W., Zhang, C., Luo, P., An, C.W., Guo, G.Q., 2016. The biosynthesis of auxin: how many paths truly lead to IAA? Plant Growth Regul. https://doi.org/10.1007/s10725-015-0103-5

Djebaili, R., Pellegrini, M., Smati, M., Del Gallo, M., Kitouni, M., 2020. Actinomycete strains isolated from saline soils: Plant-growth-promoting traits and inoculation effects on solanum lycopersicum. Sustain. 12. https://doi.org/10.3390/SU12114617

Duca, D.R., Glick, B.R., 2020. Indole-3-acetic acid biosynthesis and its regulation in plant-associated bacteria. Appl. Microbiol. Biotechnol. https://doi.org/10.1007/s00253-020-10869-5

Ebtehaj, I., Bonakdari, H., 2013. Evaluation of sediment transport in sewer using artificial neural network. Eng. Appl. Comput. Fluid Mech. 7, 382–392. https://doi.org/10.1080/19942060.2013.11015479

Esquivel, P., international, V.J.-F. research, 2012, undefined, 2012. Functional properties of coffee and coffee by-products. Elsevier 46, 488–495. https://doi.org/10.1016/j.foodres.2011.05.028

Fan, M., Hu, J., Cao, R., Ruan, W., Wei, X., 2018. A review on experimental design for pollutants removal in water treatment with the aid of artificial intelligence. Chemosphere 200, 330–343. https://doi.org/10.1016/J.CHEMOSPHERE.2018.02.111

Fan, M., Hu, J., Cao, R., Xiong, K., Wei, X., 2017. Modeling and prediction of copper removal from aqueous solutions by nZVI/rGO magnetic nanocomposites using ANN-GA and ANN-PSO. Sci. Rep. 7, 1–14. https://doi.org/10.1038/s41598-017-18223-y

Gelová, Z., Gallei, M., Pernisová, M., Brunoud, G., Zhang, X., Glanc, M., Li, L., Michalko, J., Pavlovičová, Z., Verstraeten, I., Han, H., Hajný, J., Hauschild, R., Čovanová, M., Zwiewka, M., Hoermayer, L., Fendrych, M., Xu, T., Vernoux, T., Friml, J., 2021. Developmental roles of Auxin Binding Protein 1 in Arabidopsis thaliana. Plant Sci. 303, 110750. https://doi.org/10.1016/j.plantsci.2020.110750

Ghaedi, A.M., Vafaei, A., 2017. Applications of artificial neural networks for adsorption removal of dyes from aqueous solution: A review. Adv. Colloid Interface Sci. 245, 20–39. https://doi.org/10.1016/J.CIS.2017.04.015

Ghaedi, M., Ansari, A., Bahari, F., Ghaedi, A.M., Vafaei, A., 2015a. A hybrid artificial neural network and particle swarm optimization for prediction of removal of hazardous dye brilliant green from aqueous solution using zinc sulfide nanoparticle loaded on activated carbon. Spectrochim. Acta - Part A Mol. Biomol. Spectrosc. 137, 1004–1015. https://doi.org/10.1016/j.saa.2014.08.011

Ghaedi, M., Shojaeipour, E., Ghaedi, A.M., Sahraei, R., 2015b. Isotherm and kinetics study of malachite green adsorption onto copper nanowires loaded on activated carbon: Artificial neural network modeling and genetic algorithm optimization. Spectrochim. Acta - Part A Mol. Biomol. Spectrosc. 142, 135–149. https://doi.org/10.1016/j.saa.2015.01.086

Gherbawy, Y., Elhariry, H., Altalhi, A., El-Deeb, B., Khiralla, G., 2012. Molecular screening of Streptomyces isolates for antifungal activity and family 19 chitinase enzymes. J. Microbiol. 50, 459–468. https://doi.org/10.1007/s12275-012-2095-4

Girão, M., Ribeiro, I., Ribeiro, T., Azevedo, I.C., Pereira, F., Urbatzka, R., Leão, P.N., Carvalho, M.F., 2019. Actinobacteria isolated from laminaria ochroleuca: A source of new bioactive compounds. Front. Microbiol. 10, 1–13. https://doi.org/10.3389/fmicb.2019.00683

Gómez-De La Cruz, F.J., Cruz-Peragón, F., Casanova-Peláez, P.J., Palomar-Carnicero, J.M., 2015. A vital stage in the large-scale production of biofuels from spent coffee grounds: The drying kinetics. Fuel Process. Technol. 130, 188–196. https://doi.org/10.1016/j.fuproc.2014.10.012

Gómez Ramírez, M., Rojas Avelizapa, L.I., Rojas Avelizapa, N.G., Cruz Camarillo, R., 2004. Colloidal chitin stained with Remazol Brilliant Blue R®, a useful substrate to select chitinolytic microorganisms and to evaluate chitinases. J. Microbiol. Methods 56, 213–219. https://doi.org/10.1016/J.MIMET.2003.10.011

Gonzalez-Franco, A.C., Deobald, L.A., Spivak, A., Crawford, D.L., 2003. Actinobacterial chitinase-like enzymes: Profiles of rhizosphere versus non-rhizosphere isolates. Can. J. Microbiol. 49, 683–698. https://doi.org/10.1139/w03-089

Goudjal, Y., Toumatia, O., Sabaou, N., Barakate, M., Mathieu, F., Zitouni, A., 2013. Endophytic actinomycetes from spontaneous plants of Algerian Sahara: Indole-3-acetic acid production and tomato plants growth promoting activity. World J. Microbiol. Biotechnol. 29, 1821–1829. https://doi.org/10.1007/s11274-013-1344-y

Goudjal, Y., Toumatia, O., Yekkour, A., Sabaou, N., Mathieu, F., Zitouni, A., 2014. Biocontrol of Rhizoctonia solani damping-off and promotion of tomato plant growth by endophytic actinomycetes isolated from native plants of Algerian Sahara. Microbiol. Res. 169, 59–65. https://doi.org/10.1016/j.micres.2013.06.014

Goudjal, Y., Zamoum, M., Meklat, A., Sabaou, N., Mathieu, F., Zitouni, A., 2016. Plant-growth-promoting potential of endosymbiotic actinobacteria isolated from sand truffles (Terfezia leonis Tul.) of the Algerian Sahara. Ann. Microbiol. 66, 91–100.

https://doi.org/10.1007/s13213-015-1085-2

Gravel, V., Antoun, H., Tweddell, R.J., 2007. Growth stimulation and fruit yield improvement of greenhouse tomato plants by inoculation with Pseudomonas putida or Trichoderma atroviride: Possible role of indole acetic acid (IAA). Soil Biol. Biochem. 39, 1968–1977. https://doi.org/10.1016/j.soilbio.2007.02.015

Grones, P., Abas, M., Hajný, J., Jones, A., Waidmann, S., Kleine-Vehn, J., Friml, J., 2018. PID/WAG-mediated phosphorylation of the Arabidopsis PIN3 auxin transporter mediates polarity switches during gravitropism. Sci. Rep. 8, 1–11. https://doi.org/10.1038/s41598-018-28188-1

Hao, Z., Yang, B., Jahng, D., 2018. Spent coffee ground as a new bulking agent for accelerated biodrying of dewatered sludge. Water Res. 138, 250–263. https://doi.org/10.1016/J.WATRES.2018.03.049

Hardgrove, S.J., Livesley, S.J., 2016. Applying spent coffee grounds directly to urban agriculture soils greatly reduces plant growth. Urban For. Urban Green. 18, 1–8. https://doi.org/10.1016/j.ufug.2016.02.015

Huang, J., Mei, L.H., Xia, J., 2007. Application of artificial neural network coupling particle swarm optimization algorithm to biocatalytic production of GABA. Biotechnol. Bioeng. 96, 924–931. https://doi.org/10.1002/bit.21162

Huang, W., Liu, Xingyu, Zhou, X., Wang, X., Liu, Xinyu, Liu, H., 2020. Calcium Signaling Is Suppressed in Magnaporthe oryzae Conidia by Bacillus cereus HS24. Phytopathology 110, 309—316. https://doi.org/10.1094/phyto-08-18-0311-r

Hymavathi, M., Sathish, T., Brahmaiah, P., Prakasham, R.S., 2010. Impact of carbon and nitrogen sources on L-Asparaginase production by isolated bacillus circulans (MTCC 8574): Application of saturated plackett-burman design. Chem. Biochem. Eng. Q. 24, 473–480.

Islam, E., Khan, M.T., Irem, S., 2015. Biochemical mechanisms of signaling: Perspectives in plants under arsenic stress. Ecotoxicol. Environ. Saf. 114, 126–133. https://doi.org/10.1016/J.ECOENV.2015.01.017

Jasso-Salcedo, A.B., Hoppe, S., Pla, F., Escobar-Barrios, V.A., Camargo, M.-C., Meimaroglou, D., 2017. Modeling and optimization of a photocatalytic process: Degradation of endocrine disruptor compounds by Ag/ZnO. Chem. Eng. Res. Des. 128, 174–191. https://doi.org/10.1016/j.cherd.2017.10.012

Jiang, B., Zhang, F., Sun, Y., Zhou, X., Dong, J., Zhang, L., 2014. Modeling and optimization for curing of polymer flooding using an artificial neural network and a genetic algorithm. J. Taiwan Inst. Chem. Eng. 45, 2217–2224. https://doi.org/10.1016/J.JTICE.2014.03.020

Kanimozhi, J., Moorthy, I.G., Sivashankar, R., Sivasubramanian, V., 2017. Optimization of dextran production by Weissella cibaria NITCSK4 using Response Surface

Methodology-Genetic Algorithm based technology. Carbohydr. Polym. 174, 103–110. https://doi.org/10.1016/J.CARBPOL.2017.06.021

Kaur, H., Arora, D.S., Sharma, V., 2014. Isolation, purification, and characterization of antimicrobial compound 6-[1,2-dimethyl-6-(2-methyl-allyloxy)-hexyl]-3-(2-methoxy-phenyl)-chromen-4-one from Penicillium sp. HT-28. Appl. Biochem. Biotechnol. 173, 1963–1976. https://doi.org/10.1007/S12010-014-0979-Y

Kaur, R., Kaur, S., 2021. Plant growth-promoting potential of 'Myroides gitamensis' isolated from virgin soils of Punjab. Arch. Microbiol. 203, 2551–2561. https://doi.org/10.1007/s00203-021-02231-8

Khamna, S., Yokota, A., Peberdy, J.F., Lumyong, S., 2010. Indole-3-acetic acid production by Streptomyces sp. isolated from some Thai medicinal plant rhizosphere soils. EurAsian J. Biosci. 23–32. https://doi.org/10.5053/EJOBIOS.2010.4.0.4

Khosravi-Darani, K., Zoghi, A., 2008. Comparison of pretreatment strategies of sugarcane baggase: Experimental design for citric acid production. Bioresour. Technol. 99, 6986–6993. https://doi.org/10.1016/j.biortech.2008.01.024

Kusuma, A.B., Nouioui, I., Klenk, H.P., Goodfellow, M., 2020. Streptomyces harenosi sp. nov., a home for a gifted strain isolated from Indonesian sand dune soil. Int. J. Syst. Evol. Microbiol. 70, 4874–4882. https://doi.org/10.1099/IJSEM.0.004346/CITE/REFWORKS

Lanka, S., Latha, J.N.L., 2015. Response Surface Methodology as a Statistical Tool for Fermentation Media Optimization in Lipase Production by Palm Oil Mill Effluent (POME) Isolate Emericella Nidulans NFCCI 3643. Int. J. Innov. Res. Sci. Eng. Technol. (An ISO 3297, 2535–2545. https://doi.org/10.15680/IJIRSET.2015.0404060

Lessa, E.F., Nunes, M.L., Fajardo, A.R., 2018. Chitosan/waste coffee-grounds composite: An efficient and eco-friendly adsorbent for removal of pharmaceutical contaminants from water. Carbohydr. Polym. 189, 257–266. https://doi.org/10.1016/J.CARBPOL.2018.02.018

Lim, Soon Hyuk, Se-Woong La, Thi Thuy Hang Hoang, Quang Trung Le, Soonmin Jang, Jaebum Choo, Yasser Vasseghian, Sang Jun Son, and Sang-Woo Joo. "Carbon capture and biocatalytic oxygen production of photosystem II from thylakoids and microalgae on nanobiomaterials." Bioresource Technology 368 (2023): 128279.

Lin, Q., Luo, A., Zhang, Y., Wang, Y., Liang, Z., Yuan, P., 2021. Employing Artificial Neural Networks to Predict the Performance of Domestic Sewage Treatment Terminals in the Rural Region. Math. Probl. Eng. 2021. https://doi.org/10.1155/2021/5264531

López, M.E., Rene, E.R., Boger, Z., Veiga, M.C., Kennes, C., 2017. Modelling the removal of volatile pollutants under transient conditions in a two-stage bioreactor using artificial neural networks. J. Hazard. Mater. 324, 100–109. https://doi.org/10.1016/J.JHAZMAT.2016.03.018

Maji, K., Pratihar, D.K., Nath, A.K., 2014. Laser forming of a dome shaped surface:

Experimental investigations, statistical analysis and neural network modeling. Opt. Lasers Eng. 53, 31–42. https://doi.org/10.1016/j.optlaseng.2013.08.014

Mandal, S.M., Mondal, K.C., Dey, S., Pati, B.R., 2007. Optimization of Cultural and Nutritional Conditions for Indole 3-acetic Acid (IAA) Production by a Rhizobium sp. Isolated from Root Nodules of Vigna mungo (L.) Hepper. Res. J. Microbiol. 2, 239–246. https://doi.org/10.3923/jm.2007.239.246

Mazarei, F., Jooyandeh, H., Noshad, M., Hojjati, M., 2017. Polysaccharide of caper (Capparis spinosa L.) Leaf: Extraction optimization, antioxidant potential and antimicrobial activity. Int. J. Biol. Macromol. 95, 224–231. https://doi.org/10.1016/J.IJBIOMAC.2016.11.049

Medjili, Chahinaz, Nadjem Lakhdari, Delloula Lakhdari, Abderrahmane Berchi, Nadjet Osmani, Ines Laourari, Yasser Vasseghian, and Mohammed Berkani. "Synthesis of novel PANI/PVA-NiCu composite material for efficient removal of organic dyes." Chemosphere 313 (2023): 137427.

Moghri, M., Dragoi, E.N., Salehabadi, A., Shukla, D.K., Vasseghian, Y., 2017. Effect of various formulation ingredients on thermal characteristics of PVC/clay nanocomposite foams: Experimental and modeling. E-Polymers 17, 119–128. https://doi.org/10.1515/epoly-2016-0151

Mohite, B., 2013. Isolation and characterization of indole acetic acid (IAA) producing bacteria from rhizospheric soil and its effect on plant growth. J. Soil Sci. Plant Nutr. 13, 638–649. https://doi.org/10.4067/S0718-95162013005000051

Montgomery, D.C., 2019. Design and Analysis of Experiments, 10th Edition | Wiley, Wiley.

Mourabet, M., Rhilassi, A. El, Bennani-Ziatni, M., Taitai, A., 2014. Comparative Study of Artificial Neural Network and Response Surface Methodology for Modelling and Optimization the Adsorption Capacity of Fluoride onto Apatitic Tricalcium Phosphate. Univers. J. Appl. Math. 2, 84–91. https://doi.org/10.13189/ujam.2014.020202

Murthy, N., Bleakley, B., 2012. Simplified Method of Preparing Colloidal Chitin Used For Screening of Chitinase- Producing Microorganisms. Internet J. Microbiol. 10, 1–5. https://doi.org/10.5580/2e93

Mushtaq, S., Shafiq, M., Ashraf, T., Haider, M.S., Ashfaq, M., Ali, M., 2019. Characterization of plant growth promoting activities of bacterial endophytes and their antibacterial potential isolated from citrus. J. Anim. Plant Sci. 29, 978–991.

Myo, E.M., Ge, B., Ma, J., Cui, H., Liu, B., Shi, L., Jiang, M., Zhang, K., 2019. Indole-3-acetic acid production by Streptomyces fradiae NKZ-259 and its formulation to enhance plant growth. BMC Microbiol. 2019 191 19, 1–14. https://doi.org/10.1186/S12866-019-1528-1/TABLES/4

Nafis, A., Raklami, A., Bechtaoui, N., Khalloufi, F. El, Alaoui, A. El, Glick, B.R., Hafidi, M., Kouisni, L., Ouhdouch, Y., Hassani, L., 2019. Actinobacteria from extreme niches in

morocco and their plant growth-promoting potentials. Diversity 11, 1–15. https://doi.org/10.3390/d11080139

Nakurte, I., Keisa, A., Rostoks, N., 2012. Development and validation of a reversed-phase liquid chromatography method for the simultaneous determination of indole-3-acetic acid, indole-3-pyruvic acid, and abscisic acid in Barley (Hordeum vulgare L.). J. Anal. Methods Chem. 1. https://doi.org/10.1155/2012/103575

Narayana, K.J., Peddikotla, P., Krishna, P.S.J., Yenamandra, V., Muvva, V., 2009. Indole-3-acetic acid production by Streptomyces albidoflavus. J Biol Res 11, 49–55.

Nasution, N., Zamsuri, A., Lisnawita, L., Wanto, A., 2018. Polak-Ribiere updates analysis with binary and linear function in determining coffee exports in Indonesia, in: IOP Conference Series: Materials Science and Engineering. IOP Publishing, p. 012088. https://doi.org/10.1088/1757-899X/420/1/012088

Navarro, L., Dunoyer, P., Jay, F., Arnold, B., Dharmasiri, N., Estelle, M., Voinnet, O., Jones, J.D.G., 2006. A plant miRNA contributes to antibacterial resistance by repressing auxin signaling. Science (80-.). 312, 436–439. https://doi.org/10.1126/science.1126088

Nimnoi, P., Pongsilp, N., Lumyong, S., 2010. Endophytic actinomycetes isolated from Aquilaria crassna Pierre ex Lec and screening of plant growth promoters production. World J. Microbiol. Biotechnol. 26, 193–203.

Nutaratat, P., Amsri, W., Srisuk, N., Arunrattiyakorn, P., Limtong, S., 2015. Indole-3-acetic acid production by newly isolated red yeast Rhodosporidium paludigenum. J. Gen. Appl. Microbiol. 61, 1–9. https://doi.org/10.2323/jgam.61.1

Ousaadi, M.I., Merouane, F., Berkani, M., Almomani, F., Vasseghian, Y., Kitouni, M., 2021. Valorization and optimization of agro-industrial orange waste for the production of enzyme by halophilic Streptomyces sp. Environ. Res. 201, 111494. https://doi.org/10.1016/j.envres.2021.111494

Park, S., Kim, A.L., Hong, Y.K., Shin, J.H., Joo, S.H., 2021. A highly efficient auxin-producing bacterial strain and its effect on plant growth. J. Genet. Eng. Biotechnol. 19. https://doi.org/10.1186/s43141-021-00252-w

Pascoal, A., Estevinho, L.M., Martins, I.M., Choupina, A.B., 2018. REVIEW: Novel sources and functions of microbial lipases and their role in the infection mechanisms. Physiol. Mol. Plant Pathol. https://doi.org/10.1016/j.pmpp.2018.08.003

Pasin, L.A.A.P., Abreu, M.S. de, Souza, I.P., 2011. Influence of the fungi population on the physicochemical and chemical composition of coffee (Coffea arabica L.). Food Sci. Technol. 31, 681–687. https://doi.org/10.1590/s0101-20612011000300020

Passari, A.K., Chandra, P., Zothanpuia, Mishra, V.K., Leo, V.V., Gupta, V.K., Kumar, B., Singh, B.P., 2016. Detection of biosynthetic gene and phytohormone production by endophytic actinobacteria associated with Solanum lycopersicum and their plant-growth-promoting effect. Res. Microbiol. 167, 692–705.

https://doi.org/10.1016/J.RESMIC.2016.07.001

Passari, A.K., Mishra, V.K., Gupta, V.K., Yadav, M.K., Saikia, R., Singh, B.P., 2015. In vitro and in vivo plant growth promoting activities and DNA fingerprinting of antagonistic endophytic actinomycetes associates with medicinal plants. PLoS One 10. https://doi.org/10.1371/journal.pone.0139468

Poh, P.E., Gouwanda, D., Mohan, Y., Gopalai, A.A., Tan, H.M., 2016. Optimization of Wastewater Anaerobic Digestion Using Mechanistic and Meta-heuristic Methods: Current Limitations and Future Opportunities. Water Conserv. Sci. Eng. 2016 11 1, 1–20. https://doi.org/10.1007/S41101-016-0001-3

Pridham, T.G., Gottlieb, D., 1948. The Utilization of Carbon Compounds by Some Actinomycetales as an Aid for Species Determination. J. Bacteriol. 56, 107–114.

Purama, R.K., Goyal, A., 2008. Application of response surface methodology for maximizing dextransucrase production from leuconostoc mesenteroides NRRL B-640 in a bioreactor. Appl. Biochem. Biotechnol. 151, 182–192. https://doi.org/10.1007/s12010-008-8165-8

Qin, Q., Li, G., Jin, L., Huang, Y., Wang, Y., Wei, C., Xu, Z., Yang, Z., Wang, H., Li, Y., 2020. Auxin response factors (ARFs) differentially regulate rice antiviral immune response against rice dwarf virus. PLOS Pathog. 16, e1009118. https://doi.org/10.1371/JOURNAL.PPAT.1009118

Qin, S., Wu, Z., Rasool, A., Li, C., 2012. Synthesis and characterization of slow-release nitrogen fertilizer with water absorbency: Based on poly(acrylic acid-acrylic amide)/Na-bentonite. J. Appl. Polym. Sci. 126, 1687–1697. https://doi.org/10.1002/app.37007

Rajendra, M., Jena, P.C., Raheman, H., 2009. Prediction of optimized pretreatment process parameters for biodiesel production using ANN and GA. Fuel 88, 868–875. https://doi.org/10.1016/J.FUEL.2008.12.008

Rajendran, C., Baby, A., Kumari, S., Verghese, T., 1991. An evaluation of straw-extract agar media for the growth and sporulation of Madurella mycetomatis 9–12.

Rakusová, H., Han, H., Valošek, P., Friml, J., 2019. Genetic screen for factors mediating PIN polarization in gravistimulated Arabidopsis thaliana hypocotyls. Plant J. 98, 1048–1059.

Reetha, S., Selvakumar, G., Bhuvaneswari, G., Thamizhiniyan, P., Ravimycin, T., 2014. Screening of cellulase and pectinase by using Pseudomonas fluorescens and Bacillus subtilis. Int. Lett. Nat. Sci. 8.

Ribeiro, M.H.L., Silveira, D., Ebert, C., Ferreira-Dias, S., 2003. Response surface modelling of the consumption of bitter compounds from orange juice by Acinetobacter calcoaceticus. J. Mol. Catal. B Enzym. 21, 81–88. https://doi.org/10.1016/S1381-1177(02)00144-3

Ribnicky, D.M., Cohen, J.D., Hu, W.S., Cooke, T.J., 2002. An auxin surge following fertilization in carrots: a mechanism for regulating plant totipotency. Planta 214, 505–509. https://doi.org/10.1007/S004250100639

Rosenblueth, M., Martínez-Romero, E., 2006. Bacterial endophytes and their interactions with hosts. Mol. Plant-Microbe Interact. https://doi.org/10.1094/MPMI-19-0827

Roy, S., Sengupta, S., Manna, S., Das, P., 2018. Chemically reduced tea waste biochar and its application in treatment of fluoride containing wastewater: Batch and optimization using response surface methodology. Process Saf. Environ. Prot. 116, 553–563. https://doi.org/10.1016/J.PSEP.2018.03.009

Sadeghi, A., Karimi, E., Dahaji, P.A., Javid, M.G., Dalvand, Y., Askari, H., 2012. Plant growth promoting activity of an auxin and siderophore producing isolate of Streptomyces under saline soil conditions. World J. Microbiol. Biotechnol. 28, 1503–1509. https://doi.org/10.1007/s11274-011-0952-7

Saini, D., Yadav, D., Pabbi, S., Chhabra, D., Shukla, P., 2020. Phycobiliproteins from Anabaena variabilis CCC421 and its production enhancement strategies using combinatory evolutionary algorithm approach. Bioresour. Technol. 309. https://doi.org/10.1016/j.biortech.2020.123347

Schmidt, J., Marques, M.R.G., Botti, S., Marques, M.A.L., 2019. Recent advances and applications of machine learning in solid-state materials science. npj Comput. Mater. 2019 51 5, 1–36. https://doi.org/10.1038/s41524-019-0221-0

Shirling, E.B., Gottlieb, D., 1968. Cooperative Description of Type Cultures of STREPTOMYCES III. Additional Species Descriptions from First and Second Studies. Int. J. Syst. Bacteriol. 18, 279–392. https://doi.org/10.1099/00207713-18-4-279

Shirling, E.B., Gottlieb, D., 1966. Methods for characterization of Streptomyces species. Int. J. Syst. Bacteriol. 16, 313–340. https://doi.org/10.1099/00207713-16-3-313

Sivapathasekaran, C., Mukherjee, S., Ray, A., Gupta, A., Sen, R., 2010. Artificial neural network modeling and genetic algorithm based medium optimization for the improved production of marine biosurfactant. Bioresour. Technol. 101, 2884–2887. https://doi.org/10.1016/j.biortech.2009.09.093

Slama, H. Ben, Cherif-Silini, H., Bouket, A.C., Qader, M., Silini, A., Yahiaoui, B., Alenezi, F.N., Luptakova, L., Triki, M.A., Vallat, A., Oszako, T., Rateb, M.E., Belbahri, L., 2019. Screening for fusarium antagonistic bacteria from contrasting niches designated the endophyte bacillus halotoleransas plant warden against fusarium. Front. Microbiol. 10, 1–24. https://doi.org/10.3389/fmicb.2018.03236

Smaali, A., Berkani, M., Merouane, F., Le, V.T., Vasseghian, Y., Rahim, N., Kouachi, M., 2021. Photocatalytic-persulfate- oxidation for diclofenac removal from aqueous solutions: Modeling, optimization and biotoxicity test assessment. Chemosphere 266, 129158. https://doi.org/10.1016/j.chemosphere.2020.129158

Smati, M., Kitouni, M., 2019. Diversity of actinobacteria in the marshes of Ezzemoul and Djendli in northeastern Algeria. Eur. J. Ecol. 5, 41–53. https://doi.org/10.2478/eje-2019-0009

Sohn, Seungwoon, Vu Thi Huong, Phuong-Dong Nguyen, Nguyễn Hoàng Ly, Soonmin Jang, Hyewon Lee, Cheolmin Lee et al. "Equilibria of semi-volatile isothiazolinones between air and glass surfaces measured by gas chromatography and Raman spectroscopy." Environmental Research 218 (2023): 114908.

Spaepen, S., Vanderleyden, J., Remans, R., 2007. Indole-3-acetic acid in microbial and microorganism-plant signaling. FEMS Microbiol. Rev. https://doi.org/10.1111/j.1574-6976.2007.00072.x

Sreevidya, M., Gopalakrishnan, S., Kudapa, H., Varshney, R.K., 2016. Exploring plant growth-promotion actinomycetes from vermicompost and rhizosphere soil for yield enhancement in chickpea. Brazilian J. Microbiol. 47, 85–95. https://doi.org/10.1016/J.BJM.2015.11.030

Sridevi, M., Yadav, N.C.S., Mallaiah, K. V., 2008. Production of indole acetic acid by Rhizobium isolates from Crolataria species. Res J Microbiol 3, 276–281. https://doi.org/10.3923/jm.2008.276.281

Stach, N., Kaszycki, P., Wladyka, B., Dubin, G., 2018. Extracellular Proteases of Staphylococcus spp., in: Pet-to-Man Travelling Staphylococci: A World in Progress. pp. 135–145. https://doi.org/10.1016/B978-0-12-813547-1.00011-X

Suárez-Moreno, Z.R., Vinchira-Villarraga, D.M., Vergara-Morales, D.I., Castellanos, L., Ramos, F.A., Guarnaccia, C., Degrassi, G., Venturi, V., Moreno-Sarmiento, N., 2019. Plant-growth promotion and biocontrol properties of three Streptomyces spp. isolates to control bacterial rice pathogens. Front. Microbiol. 10. https://doi.org/10.3389/FMICB.2019.00290

Talhi, I., Dehimat, L., Jaouani, A., Cherfia, R., Berkani, M., Almomani, F., Vasseghian, Y., Chaouche, N.K., 2022. Optimization of thermostable proteases production under agro-wastes solid-state fermentation by a new thermophilic Mycothermus thermophilus isolated from a hydrothermal spring Hammam Debagh, Algeria. Chemosphere 286, 131479. https://doi.org/10.1016/j.chemosphere.2021.131479

Talukdar, S., Talukdar, M., Buragohain, M., Yadav, A., Yadav, R.N.S., Bora, T.C., 2016. Enhanced candicidal compound production by a new soil isolate Penicillium verruculosum MKH7 under submerged fermentation. BMC Microbiol. 16. https://doi.org/10.1186/s12866-016-0713-8

Tamura, K., Stecher, G., Kumar, S., 2021. MEGA11: Molecular Evolutionary Genetics Analysis Version 11. Mol. Biol. Evol. 38, 3022–3027. https://doi.org/10.1093/molbev/msab120

Thakur, D., Yadav, A., Gogoi, B.K., Bora, T.C., 2007. Isolation and screening of Streptomyces in soil of protected forest areas from the states of Assam and Tripura, India, for antimicribial metabolites. J. Mycol. Med. 17, 242–249. https://doi.org/10.1016/j.mycmed.2007.08.001

Toumatia, O., Compant, S., Yekkour, A., Goudjal, Y., Sabaou, N., Mathieu, F., Sessitsch, A.,

Zitouni, A., 2016. Biocontrol and plant growth promoting properties of Streptomyces mutabilis strain IA1 isolated from a Saharan soil on wheat seedlings and visualization of its niches of colonization. South African J. Bot. 105, 234–239.

Tran, Huynh Nhu, Nguyen Binh Nguyen, Nguyễn Hoàng Ly, Sang-Woo Joo, and Yasser Vasseghian. "Core-shell Au@ ZIF-67-based pollutant monitoring of thiram and carbendazim pesticides." Environmental Pollution 317 (2023): 120775.

Turan, M., Nikerel, E., Kaya, K., Kitir, N., Gunes, A., Mokhtari, N.E.P., Tüfenkçi, S., Karaman, M.R., Çimrin, K.M., 2017. Enzyme Dynamic in Plant Nutrition Uptake and Plant Nutrition, in: Enzyme Inhibitors and Activators. https://doi.org/10.5772/66938

van der Aart, L.T., Nouioui, I., Kloosterman, A., Igual, J.M., Willemse, J., Goodfellow, M., van Wezel, G.P., 2019. Polyphasic classification of the gifted natural product producer streptomyces roseifaciens sp. Nov. Int. J. Syst. Evol. Microbiol. 69, 899–908. https://doi.org/10.1099/ijsem.0.003215

Vasseghian, Y., Ahmadi, M., Joshaghani, M., 2017. Ultrasound Assisted Ash and Sulphur Removal from Bitumen Using Column Flotation Technique: Experimental, RSM and ANN Methods in Modelling and Optimization of Process. Iran. J. Sci. Technol. Trans. A Sci. 41, 1149–1163. https://doi.org/10.1007/s40995-016-0068-x

Vasseghian, Y., Bahadori, A., Khataee, A., Dragoi, E.N., Moradi, M., 2020. Modeling the Interfacial Tension of Water-Based Binary and Ternary Systems at High Pressures Using a Neuro-Evolutive Technique. ACS Omega 5, 781–790. https://doi.org/10.1021/acsomega.9b03518

Vasseghian, Y., Berkani, M., Almomani, F., Dragoi, E.N., 2021. Data mining for pesticide decontamination using heterogeneous photocatalytic processes. Chemosphere 270, 129449. https://doi.org/10.1016/j.chemosphere.2020.129449

Vasseghian, Y., Dragoi, E.-N., 2018. Modeling and Optimization of Acid Blue 193 Removal by UV and Peroxydisulfate Process. J. Environ. Eng. 144, 06018003. https://doi.org/10.1061/(asce)ee.1943-7870.0001405

Verma, V.C., Gond, S.K., Kumar, A., Mishra, A., Kharwar, R.N., Gange, A.C., 2009. Endophytic actinomycetes from azadirachta indica A. Juss.: Isolation, diversity, and anti-microbial activity. Microb. Ecol. 57, 749–756. https://doi.org/10.1007/s00248-008-9450-3

Vranova, V., Rejsek, K., Formanek, P., 2013. Proteolytic activity in soil: A review. Appl. Soil Ecol. https://doi.org/10.1016/j.apsoil.2013.04.003

Williams, S.T., Goodfellow, M., Wellington, E.M.H., Vickers, J.C., Alderson, G., Sneath, P.H., Sackin, M.J., Mortimer, A.M., 1983. A probability matrix for identification of some streptomycetes. J. Gen. Microbiol. 129, 1815–1830. https://doi.org/10.1099/00221287-129-6-1815

Wu, C., Agrawal, D.C., Huang, W., Hsu, H., Yang, S., Huang, S., Lin, Y., 2019. Functionality

Analysis of Spent Coffee Ground Extracts Obtained by the Hydrothermal Method 2019.

Xu, T., Li, Y., Zeng, X., Yang, X., Yang, Y., Yuan, S., Hu, X., Zeng, J., Wang, Z., Liu, Q., Liu, Y., Liao, H., Tong, C., Liu, X., Zhu, Y., 2017. Isolation and evaluation of endophytic Streptomyces endus OsiSh-2 with potential application for biocontrol of rice blast disease. J. Sci. Food Agric. 97, 1149–1157. https://doi.org/10.1002/jsfa.7841

Yahya, H.S.M., Abbas, T., Amin, N.A.S., 2020. Optimization of hydrogen production via toluene steam reforming over Ni–Co supported modified-activated carbon using ANN coupled GA and RSM. Int. J. Hydrogen Energy 46, 24632–24651. https://doi.org/10.1016/J.IJHYDENE.2020.05.033

Yan, T., Id, Y., Feng, R.J., Zhou, D.B., Pan, Y.Y., Chen, Y.F., Wang, F., Yin, L.Y., Zhang, Y.D., Xie, J.H., 2018. Optimization of fermentation conditions through response surface methodology for enhanced antibacterial metabolite production by Streptomyces sp . 1-14 from cassava rhizosphere. PLoS One 1–14.

Yetilmezsoy, K., Demirel, S., 2008. Artificial neural network (ANN) approach for modeling of Pb(II) adsorption from aqueous solution by Antep pistachio (Pistacia Vera L.) shells. J. Hazard. Mater. 153, 1288–1300. https://doi.org/10.1016/J.JHAZMAT.2007.09.092

Zamoum, M., Goudjal, Y., Sabaou, N., Barakate, M., Mathieu, F., Zitouni, A., 2015. Biocontrol capacities and plant growth-promoting traits of endophytic actinobacteria isolated from native plants of Algerian sahara. J. Plant Dis. Prot. 122, 215–233. https://doi.org/10.1007/bf03356555

Zhang, Y., Pan, B., 2014. Modeling batch and column phosphate removal by hydrated ferric oxide-based nanocomposite using response surface methodology and artificial neural network. Chem. Eng. J. 249, 111–120. https://doi.org/10.1016/j.cej.2014.03.073

Zhao, J., Wang, X., Sun, W., Mou, Y., Peng, Y., Zhou, L., 2013. Medium optimization for palmarumycin C13 production in liquid culture of endophytic fungus Berkleasmium sp. Dzf12 using response surface methodology. Electron. J. Biotechnol. 16, 16. https://doi.org/10.2225/vol16-issue6-fulltext-10

Zhou, X., Wang, J.T., Zhang, Z.F., Li, W., Chen, W., Cai, L., 2020. Microbiota in the Rhizosphere and Seed of Rice From China, With Reference to Their Transmission and Biogeography. Front. Microbiol. 11, 1–13. https://doi.org/10.3389/fmicb.2020.00995